applied sciences

MDPI

Article

Chemical-Inspired Material Generation Algorithm (MGA) of Single- and Double-Diode Model Parameter Determination for Multi-Crystalline Silicon Solar Cells

Wafaa Alsaggaf [1], Mona Gafar [2,3], Shahenda Sarhan [4,5], Abdullah M. Shaheen [6,*] and Ahmed R. Ginidi [6]

1 Department of Information Technology, Faculty of Computing and Information Technology, King Abdulaziz University, Jeddah 21589, Saudi Arabia; waalsaggaf@kau.edu.sa
2 Department of Computer Engineering and Information, College of Engineering, Wadi Ad Dwaser, Prince Sattam Bin Abdulaziz University, Al-Kharj 16278, Saudi Arabia; m.gafar@psau.edu.sa
3 Machine Learning and Information Retrieval Department, Artificial Intelligence Kafrelsheikh University, Kafrelsheikh 33516, Egypt
4 Computer Science Department, Faculty of Computers and Information, Mansoura University, Mansoura 35516, Egypt; sh_sarhan@mans.edu.eg
5 University of Economics and Human Sciences, 01-043 Warsaw, Poland
6 Department of Electrical Engineering, Faculty of Engineering, Suez University, Suez P.O. Box 43221, Egypt; ahmed.ginidi@eng.suezuni.edu.eg
* Correspondence: abdullah.mohamed.eng19@suezuni.edu.eg

Abstract: The optimization of solar photovoltaic (PV) cells and modules is crucial for enhancing solar energy conversion efficiency, a significant barrier to the widespread adoption of solar energy. Accurate modeling and estimation of PV parameters are essential for the optimal design, control, and simulation of PV systems. Traditional optimization methods often suffer from limitations such as entrapment in local optima when addressing this complex problem. This study introduces the Material Generation Algorithm (MGA), inspired by the principles of material chemistry, to estimate PV parameters effectively. The MGA simulates the creation and stabilization of chemical compounds to explore and optimize the parameter space. The algorithm mimics the formation of ionic and covalent bonds to generate new candidate solutions and assesses their stability to ensure convergence to optimal parameters. The MGA is applied to estimate parameters for two different PV modules, RTC France and Kyocera KC200GT, considering their manufacturing technologies and solar cell models. The significant nature of the MGA in comparison to other algorithms is further demonstrated by experimental and statistical findings. A comparative analysis of the results indicates that the MGA outperforms the other optimization strategies that previous researchers have examined for parameter estimation of solar PV systems in terms of both effectiveness and robustness. Moreover, simulation results demonstrate that MGA enhances the electrical properties of PV systems by accurately identifying PV parameters under varying operating conditions of temperature and irradiance. In comparison to other reported methods, considering the Kyocera KC200GT module, the MGA consistently performs better in decreasing RMSE across a variety of weather situations; for SD and DD models, the percentage improvements vary from 8.07% to 90.29%.

Keywords: material generation algorithm; PV parameters estimation; single-diode model; double-diode model; various weather conditions

check for updates

Citation: Alsaggaf, W.; Gafar, M.; Sarhan, S.; Shaheen, A.M.; Ginidi, A.R. Chemical-Inspired Material Generation Algorithm (MGA) of Single- and Double-Diode Model Parameter Determination for Multi-Crystalline Silicon Solar Cells. *Appl. Sci.* **2024**, *14*, 8549. https://doi.org/10.3390/app14188549

Academic Editors: Francesco Enrichi, Enrico Trave and Elti Cattaruzza

Received: 29 July 2024
Revised: 13 September 2024
Accepted: 18 September 2024
Published: 23 September 2024

Copyright: © 2024 by the authors. Licensee MDPI, Basel, Switzerland. This article is an open access article distributed under the terms and conditions of the Creative Commons Attribution (CC BY) license (https://creativecommons.org/licenses/by/4.0/).

1. Introduction

1.1. Challenges in Photovoltaic (PV) System Efficiency and Parameter Estimation

Environmental degradation and the energy crises are becoming worse because of global industrialization. Renewable and non-polluting energy sources are thought to be promising substitute energy sources to address these issues [1]. Due to its high-power generation efficiency, ease of installation, and accessibility, solar energy has become popular

in many different countries. Nevertheless, a photovoltaic (PV) system's power output is severely limited by underutilization, malfunctions, and weather-related reliance. When PV systems are operated in unfavorable circumstances, the PV modules may gradually deteriorate, reducing the system's efficiency. The parameter values determine how accurate the mathematical models are when simulating PV modules. Even if the manual tables supplied by the PV cell manufacturers cover a lot of characteristics, there are still a lot of crucial factors that are unknown or change depending on the working environment, and there is no new measurement technology available. Thus, simulating the behavior of a real PV cell by determining unidentified parameters by means of multiple approaches, which involves fitting their actual measured I–V data under all operating conditions, is a widely used model for precisely modeling a PV system under various circumstances of operation [2].

1.2. Advanced PV Technologies with Distinct Efficiencies

PV solar cells are pivotal in harnessing solar energy to generate electricity, with their efficiency and effectiveness closely tied to the materials used in their construction. Among these, silicon (Si) remains the most prevalent, categorized into monocrystalline, polycrystalline, and amorphous types [3]. Monocrystalline Si cells are widely used in commercial applications, while polycrystalline cells offer a more cost-effective option with slightly lower performance. Amorphous Si cells, utilized in thin-film technologies, are flexible and lightweight but generally have lower efficiency. Thin-film solar cells, made from materials like cadmium telluride (CdTe), copper indium gallium selenide (CIGS), and amorphous Si, provide alternatives with their own advantages, such as reduced production costs and flexibility [4]. Perovskite (PVK) materials, such as methylammonium lead iodide (MAPbI3), have recently garnered attention for their high efficiency and low production costs, though their stability and scalability remain areas of active research [5]. Additionally, emerging technologies like organic PVs and quantum dot (QD) solar cells are being explored [6] for their potential to offer flexible, lightweight solutions and enhanced light absorption. Innovations in material properties, such as multi-junction cells and hybrid materials, continue to drive advancements in solar technology, but challenges such as stability, environmental impact, and large-scale manufacturing need to be addressed.

The promise of Si photonics technological advances to provide high-performance, small, photonic-integrated circuits has attracted a lot of interest over the past few years. The incorporation of germanium (Ge-) or III–V material-based avalanche photodiodes (APDs) on Si photonics platforms provides very sensitive optical receivers for communication wavelengths [7]. APDs integrated on Si across multiple material systems, such as Si–germanium (Si–Ge), indium gallium arsenide–indium aluminum arsenide (InGaAs–InAlAs), indium arsenide QD (InAs QD), and indium arsenide–gallium arsenide QD (InAs–GaAs QD) structures, highlight distinct performance characteristics. Currently the most sophisticated, Si–Ge APDs have low breakdown voltages and large bandwidth because of their narrow multiplication areas, and they are perfect for high bit-rate operations because Si naturally has little excess noise. APDs based on III–V semiconductors, on the other hand, were merged utilizing either monolithic or heterogeneous techniques, in spite of their substantial lattice mismatch with Si. This lattice mismatch results in greater dark currents for bulk InGaAs–InAlAs systems grown on Si; however, some of these problems have been alleviated by the insertion of buffer layers [7]. As a viable substitute, InAs QD devices enable substantial dark current reduction and strong charge localization that increases resistance to faults. Similar to this, heterojunctions with intrinsic thin layers (HITs) structures have emerged in Si solar cells as a popular option among the top technologies. Improving the efficiency of these cells by 26.45% when illuminated from the top and 21.21% when illuminated from the back has been achieved utilizing the emitter a-Si:H(n) layer in p-type bifacial HIT solar cells [8]. PVK solar cells have drawn a lot of interest lately because of their constantly rising power conversion efficiency, easy solution production method, flyability, low weight, wearability, and inexpensive material components. Due to the development of appropriate

interface and electrode materials, together with the production of high-quality PVK films made possible by low-temperature synthesis processes, the efficiency of PVK solar cells has exceeded 25% in recent years [9]. Additionally, the PVK cells have been upgraded through the application of metallic nanoparticles, leveraging the plasmonic effect. In p–n junction cells, metallic nanoparticles primarily enhance the optical plasmonic effect by aiding in photon capture. In [10], the chemical composition of the PVK has been adjusted, and the design of the metallic nanoparticles has been customized, focusing specifically on bi-metallic multi-shell elongated nanoparticles with double plasmon resonance.

Consequently, self-assembled monolayers (SAMs) have become a viable organic material for bridging PVK and metal oxides (MOs) to improve interface passivation, adjust energy levels, and stop chemical corrosion, all of which contribute to improved cell performance [11]. The deposition techniques, molecular structure, and potential of SAMs in narrow-band gap PVK solar cells set them apart and are thought to be essential for PVK solar cell improvements in the solar PV industry in the future. In order to improve the effectiveness of the cells by creating an extra electrical field that facilitates charge production, transport, and collection, ferroelectric PVK solar cells are also being evaluated as halide PVKs. PVK composites, including intrinsic ferroelectric, micro phase-separated, and layer-structured, had been three different categories into which they were divided according to the degree of phase segregation [12]. These configurations greatly increase the efficiency of solar cells while providing a variety of optoelectronic features. Moreover, PVK/Si tandem solar cells have demonstrated remarkable achievement in solar energy production, surpassing the theoretical maximum of single-junction cells by achieving a validated conversion rate of 33.9%, thanks to advances in the surface texturing of Si bottom cells [13]. Silver Bismuth Iodide ($AgBi_2I_7$) thin films were also showing promise as materials for heterojunction UV photodetectors because of their outstanding optoelectronic qualities and stability in the environment [14]. Featuring an entire width at half its maximum of around 30 nm, the films had been effectively constructed on wide-bandgap Gallium Nitride (GaN) to produce an $AgBi_2I_7$/GaN heterojunction that demonstrated robust UV–A ray detection, displaying high-performance UV photodetectors. Several other compositions were merged to the PVK solar cells to improve its efficiency, such as ammonium hexafluorophosphate (NH_4PF_6) [15], Poly(3-hexylthiophene) (P3HT) [16], and magnetron-sputtered molybdenum rear electrodes [17].

1.3. PV Cell Electrical Modelling via Optimization Algorithms

On the other hand, PV cell electrical modeling is essential for maximizing their performance and successfully incorporating them into power systems. Such models give researchers and engineers a comprehensive picture of the electrical properties and behavior of PV cells, allowing them to forecast a solar panel's performance in different scenarios. Precise electrical models play a crucial role in the design and assessment of photovoltaic systems because they facilitate the knowledge and mitigation of several issues, including aging, shading, and temperature fluctuations, that impact energy output [18]. Electrical models, in particular, make it easier to simulate PV cell I–V (current–voltage) characteristics, which are essential for determining the cells' efficiency and dependability. The characteristics that collectively characterize the performance of the cell are commonly included in these models, and they include things like fill factor, open-circuit voltage, short-circuit current, and series and parallel resistances [19]. A few instances of the several electrical models that have been examined in the literature include the single-diode (SD) model [20] and the double-diode (DD) model [21]. The literature contains a wide range of approaches of different categories in handling these equivalent circuit representations. Analytical techniques use mathematical formulas to determine the unknown parameters [22]. It is possible to broadly classify the many approaches used to derive the assessment parameters for PV models into two categories: analytical methods and Natural-inspired metaheuristics. Analytical techniques include the Lambert W function [23] and the Newton–Raphson [24].

Numerous scholars are delving into the challenging task of pinpointing the unknown parameters within the PV model due to its multifaceted nature characterized by multiple parameters, nonlinearity, and nonconvexity. In recent years, natural-inspired metaheuristics (NiMH) optimization approaches have been widely used to handle PV system parameter estimate problems, and they have been shown to perform better than conventional methods. These methods imply Particle Swarm Optimizer (PSO) [25], teaching–learning-based optimizer [26], genetic algorithm [27], seagull optimization algorithm [28], differential evolution [29], biogeographic-based optimizer [30], supply–demand optimization [31], bonobo optimizer [32], sunflower algorithm [33], Marine Predator Algorithm (MPA) [34], butterfly optimization algorithm [35], and social networking search technique [36]. The NiMH approaches can effectively handle optimization and analysis challenges because they function as a black box with no restrictions on the issue formulation. This provides NiMH with several distinct features over other techniques. Thus, to address the parametric problems with solar PV cell models, researchers have recently used a range of NiMH [37]. However, most optimization methods identified in the scientific literature have some drawbacks. For instance, an enhanced version of the generalized normal distribution algorithm (GNDA) was presented in [38] in order to model PV system behaviors. In order to enhance the GNDA's performance, two other processes—a premature convergence process and a ranking-based update—were added in this work; however, this mechanism resulted in a computing load that was twice as great as that of the GNDA itself. Additionally, the memetic-adapted differential evolution algorithm did not perform well when interacting with the DD-mode formulation in [39].

1.4. Material Generation Algorithm (MGA) and Major Contributions

Material Generation Algorithm (MGA) is a novel comprehensive optimization framework inspired by the principles of material chemistry [40]. The purpose of the MGA is to increase the effectiveness of exploration and exploitation in the search space by simulating the creation and stabilization of chemical compounds to explore and optimize the parameter space. The algorithm mimics the formation of ionic and covalent bonds to generate new candidate solutions and assesses their stability to ensure convergence to optimal parameters. MGA is applied to estimate parameters for RTC France and Kyocera KC200GT PV modules, considering their manufacturing technologies and solar cell models. The root-mean-square error between the experimental values and the partially estimated model current is considered as the fitness function.

The key findings of this study are as follows:

- A proposed MGA is introduced for the first time to solve the PV parameter estimation issue.
- The efficacy of the algorithm is evaluated by the SD and DD models, demonstrating an outstanding consistency between the simulated and actual data.
- The suggested MGA exhibits noteworthy benefits and resilience in comparison to previous findings documented for both PV modules.
- MGA improves the electrical characteristics of PV systems by precisely determining the PV parameters under various temperature and irradiance operating circumstances.

2. Problem Formulation and Mathematical Model for PV Parameters Extraction

The mathematical model of solar PV cells is introduced in this section, along with the formulation of the optimization problem to extract unknown parameters. A diode exposed to sunlight can be thought of as a solar cell. The electrical behavior of a solar cell is typically modeled using the Shockley-diode equivalent circuit [41]. Despite the fact that an ideal solar cell is modeled as a photocurrent source connected in parallel to an ideal diode, the lack of an ideal source in real life causes the model's analysis to differ greatly from the results of actual I–V characteristics. Consequently, for accurate modeling of solar PV cells, non-ideal behavior, such as the impact of series and parallel resistance with conduction phenomena, must be taken into account. Although there are various PV models available,

the SD and DD models are frequently used in the literature to express the I–V characteristics of a solar cell.

2.1. SD Model

The solar cell exposed to sunlight is represented in the equivalent circuit design of a SD as a diode, a photocurrent source, and two parasitic resistors. Temperature and solar light produce the photocurrent (I_{ph}). An obstruction to current flow is represented by a lumped-series resistance (R_{ss}), which is made up of the electrode resistance, contact resistance, and material bulk resistance. The leakage current across the p–n junction is measured by the shunt resistance (R_{sh}). In a real solar cell, the diode (D) has a modified diode ideality factor to account for the combined influence of conduction processes. A quality metric used to determine how closely a practical solar cell resembles an ideal solar cell is the ideality factor, whose value is dependent on semiconductor material and manufacturing process. The equivalent circuit diagram of a SD model is illustrated in Figure 1. Using Kirchhoff's current law (KCL), the solar cell's current can be stated as follows [42]:

$$I = I_{ph} - I_{S1}\left[\exp\left(\frac{IR_{ss} + V_t}{\eta_1 V_{th}}\right) - 1\right] - \left(\frac{IR_{ss} - V_t}{R_{sh}}\right) \quad (1)$$

where V_t is the terminal voltage, and η_1 and I_{S1} stand for the ideality factor and reverse saturated current associated with the diode (D1). The thermal voltage of the PV cell is represented by V_{th}, which could be computationally characterized as indicated by Equation (2):

$$V_{th} = \frac{K_{BZ}T}{q_c} \quad (2)$$

where T and k stand for the cell temperature in Kelvin and Boltzmann's constant ($1.3806503 \times 10^{-23}$ J/K). The Shockley diode equation uses q_c ($1.60217646 \times 10^{-19}$) to represent the electron's charge magnitude.

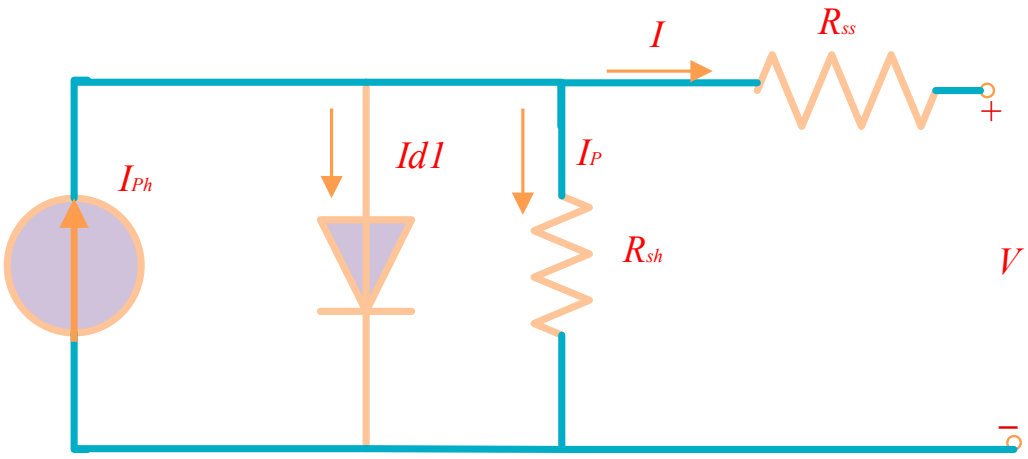


Figure 1. Schematic diagram of the PV circuit regarding the SD model.

From the measured I–V data of solar cells, five unknown parameters (X = [I_{ph}, R_{ss}, n, I_{S1}, R_{sh}]) in Equation (1) must be determined. The precise choice of these factors has a significant impact on a solar cell's performance. To illustrate, the SD model can be used to determine the maximum conversion efficiency if the parameters are chosen accurately.

2.2. DD Model of PV

The DD model's equivalent circuit design is displayed in Figure 2. Diode (D2) replicates carrier recombination in the space charge region of the junction, while diode (D1) depicts the minority charge carriers' diffusion process. Diffusion and recombination current

components are represented by the currents I_{S1} and I_{S2}, respectively. The DD model's I–V characteristic curve can be described as follows by using KCL:

$$I = I_{ph} - I_{S1}\left[\exp\left(\frac{IR_{ss}+V_t}{\eta_1 V_{th}}\right)-1\right] - I_{S2}\left[\exp\left(\frac{IR_{ss}+V_t}{\eta_2 V_{th}}\right)-1\right] - \frac{IR_{ss}}{R_{sh}} + \frac{V_t}{R_{sh}} \quad (3)$$

where the ideality factor and reverse saturation current pertaining to the diode (D2), respectively, are represented by η_2 and I_{S2}.

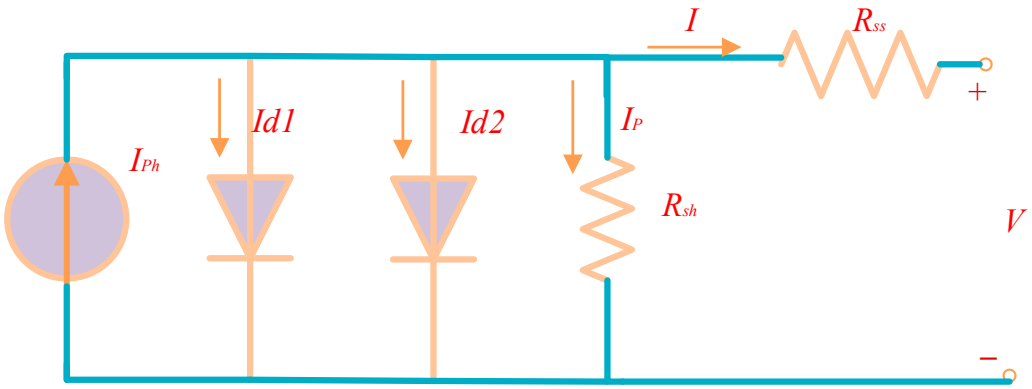


Figure 2. Schematic diagram of the PV circuit regarding the DD model.

From the measured I–V data of solar cells, seven unknown parameters ($X = [I_{ph}, R_{ss}, \eta_1, \eta_2, I_{s1}, I_{S2}, R_{sh}]$) in Equation (3) must be determined. The precise choice of these factors has a significant impact on a solar cell's performance. To illustrate, the DD model can be used to determine the maximum conversion efficiency if the parameters are chosen accurately.

2.3. PV Modules Handling

To illustrate the equations of the SD and DD models, consider a PV module consisting of N_{ss} cells connected in series and N_{pl} cells linked in parallel. Consequently, Equations (1) and (3) for the SD and DD models are refined and modified to become 4 and 5 in the following way:

$$I = N_{pl}\left(I_{ph} - I_{S1}\left[\exp\left(\frac{1}{\eta_1 N_{ss} V_{th}} \times \left(\frac{IN_{ss}R_{ss}+V_t}{N_{pl}}\right)\right)-1\right]\right) - \frac{1}{N_{ss}N_{pl}R_{sh}} \times \left(\frac{IN_{ss}R_{ss}+V_t}{N_{pl}}\right) \quad (4)$$

$$I = N_{pl}\left(\begin{array}{l} I_{ph} - I_{S1}\left[\exp\left(\frac{1}{\eta_1 N_{ss} V_{th}} \times \left(\frac{IN_{ss}R_{ss}+V_t}{N_{pl}}\right)\right)-1\right] \\ -I_{S2}\left[\exp\left(\frac{1}{\eta_2 N_{ss} V_{th}} \times \left(\frac{IN_{ss}R_{ss}+V_t}{N_{pl}}\right)\right)-1\right] \end{array}\right) - \frac{1}{N_{ss}N_{pl}R_{sh}} \times \left(\frac{IN_{ss}R_{ss}+V_t}{N_{pl}}\right) \quad (5)$$

Optimization techniques including the proposed MGA are used to compute variables that are not taken into account in the PV cell or module for the PVSD and PVDD models.

2.4. Objective Model

The statistical analysis in this article, which focused on the root mean square error (*RMSE*), is conducted using the following equation [43]:

$$RMSE = \sqrt{\frac{1}{MP}\left(\sum_{L=1}^{MP}\left(I^L_{calc}(V^L_{t,exp\ n}, x) - I^L_{exp\ n}\right)^2\right)} \quad (6)$$

where MP indicates the number of measured data points, $I^L_{exp\ n}$ and $V^L_{exp\ n}$ characterize the observed current and voltage, and x indicates the searching individual and comprises the potential PV characteristics.

3. Designed MGA for Parameter Determination for Multi-Crystalline Silicon Solar Cells

The MGA is an innovative metaheuristic approach inspired by the principles of material chemistry. It mimics the processes involved in creating and refining new materials to enhance their properties. The algorithm is built upon fundamental concepts from material chemistry, including the formation of compounds, chemical reactions, and achieving stability. By integrating these principles, the MGA provides a distinctive and effective method for addressing complex optimization challenges.

3.1. MGA Conceptual Inspiration

3.1.1. Chemical Compound

Ionic compounds are formed through the transfer of electrons from one element to another, resulting in ions that are held together by electrostatic forces. For instance, sodium chloride (NaCl) is created when a sodium atom donates an electron to become a sodium cation (Na^+), while a chlorine atom accepts the electron to become a chloride anion (Cl^-). Conversely, covalent compounds arise when atoms share electrons, typically between nonmetals. A prime example of this is the hydrogen molecule (H_2), which forms when two hydrogen atoms share electrons, resulting in a stable covalent bond.

3.1.2. Chemical Reaction

Chemical reactions are processes in which substances, known as reactants, are transformed into different substances, called products. This transformation involves the breaking and forming of chemical bonds, resulting in changes in the composition and properties of the substances involved. Chemical reactions are fundamental to the understanding of chemistry and are responsible for a vast array of natural and industrial processes. Chemical reactions transform materials into new products with distinct properties.

3.1.3. Chemical Stability

Chemical stability is a critical factor in the creation of materials, as it pertains to their ability to withstand changes, such as decomposition or reactions, when subjected to different conditions. Materials that exhibit stability are capable of retaining their properties over time, indicating resistance to degradation or alteration. In contrast, unstable materials are prone to decomposition or reaction, making them susceptible to changes in their composition or properties under varying environmental or chemical conditions.

3.2. Mathematical Model

The MGA is an optimization algorithm that incorporates the fundamental concepts of chemical compounds, reactions, and stability. It leverages these principles to formulate an effective approach for solving optimization problems. In this algorithm, a population of materials, or solutions, is taken into consideration. These materials are composed of elements from the periodic table, which serve as the decision variables within the optimization model.

3.2.1. Initialization

Each material (MT_k) is a combination of elements ($X_{k,1}\ X_{k,2}\ X_{k,3} \ldots\ldots\ldots\ldots\ X_{k,Dim}$) as displayed in Equation (7) where each element symbolized by (X) refers to one decision variable of the whole set of decision variables with number (D). Also, the number of materials represents the population size of (N_{MT}).

$$MT_k = [X_{k,1}\ X_{k,2}\ X_{k,3} \ldots\ldots\ldots\ldots\ X_{k,D}], \qquad k = 1 : N_{MT} \tag{7}$$

In order to initial their values, Equation (8) can be utilized to randomly determine each value within defined bounds.

$$MT_k(It = 0) = Low_k + R1_k \times (Up_k - Low_k), \qquad k = 1 : N_{MT} \tag{8}$$

where, It refers to the iteration value and the number (0) refers to the initial population, Up_k and Low_k indicate the upper and lower limits of each decision variable (k). $R1$ is a randomized generated number regarding each decision variable (k).

3.2.2. Modeling Chemical Compound

Elements can lose, gain, or share electrons to form new materials. To model the behavior of these ionic and covalent compounds, a selection is made of d random elements using an initial matrix (Equation (7)). The processes of electron loss, gain, or sharing for the selected elements are then simulated using probability theory. To accomplish this, a continuous probability distribution is employed for each element, allowing for the configuration of a chemical compound. This resulting compound is considered as a new element in the modeling process as follows:

$$X_{k,j}(It+1) = X_{Rd1,Rd2}(It) + e^{-}, \qquad k = 1 : N_{MT}; j = 1 : D \tag{9}$$

Here, $Rd1$ and $Rd2$ denote randomly distributed integers drawn from a uniform distribution, while e^{-} symbolizes the stochastic element represented by a normal Gaussian distribution.

Utilizing a normal Gaussian distribution, the probabilistic calculation of e^{-} is employed. This method outlines the probability of choosing a new element $X_{k,j}(It+1)$ relative to the randomly selected initial element $X_{Rd1,Rd2}(It)$ from the current iteration as follows:

$$f\left(X_{k,j}\middle|\mu,\sigma^2\right) = \left(\frac{1}{2\pi\sigma^2}\right) \times e^{\frac{-(x-\mu)^2}{(2\sigma^2)}} \tag{10}$$

In this context, μ signifies the statistical parameter representing the mean, median, or expectation of the distribution linked to the selected random element ($X_{Rd1,Rd2}(It)$). σ refers to the standard deviation, a measure of the dispersion of data points from the mean, which is standardized to unity in this paper. Furthermore, σ^2 represents the variance, while e represents the base of the natural logarithm, often referred to as the natural or Naperian base.

3.2.3. Modeling Chemical Reaction

To mathematically depict the generation of new materials via chemical reactions, an integer random number (IN) is first determined, indicating the count of materials from the current population ($MT(It)$) that will participate in the reaction. Subsequently, IN random integers (IV) are generated to denote the positions of the selected materials within the current population ($MT(It)$), forming new solutions as linear combinations of others. Additionally, a participation factor (ψ) is calculated for each material, reflecting their varying degrees of involvement in the reactions.

$$MT_k(It+1) = \left(\sum_{i=1}^{IN} \psi_i \times MT_i(It)\right) / \left(\sum_{i=1}^{IN} \psi_i\right), \qquad k = 1 : N_{MT} \tag{11}$$

Here, the current set is (MT_i). Gaussian distribution corresponding to the participation factor of the ith material, and $MT_k(It+1)$ denotes the new material resulting from the chemical reaction concept.

3.2.4. Modeling Chemical Stability

The concept of material stability involves the natural inclination of systems to achieve both local and general equilibrium across all structural levels. It can be mathematically modeled by evaluating the quality of solutions. It is essential to evaluate the stability levels of both the initial materials and the newly produced materials to determine their inclusion in the overall material list (MT) representing the solution candidates. The new solution candidates' quality is then compared to the initial ones, with the new materials replacing the initial materials that exhibit the worst fitness values and stability levels.

The flowchart in Figure 3 summarizes the MGA process, illustrating the sequence of generating new materials, evaluating their stability, and updating the population to achieve optimized solutions.

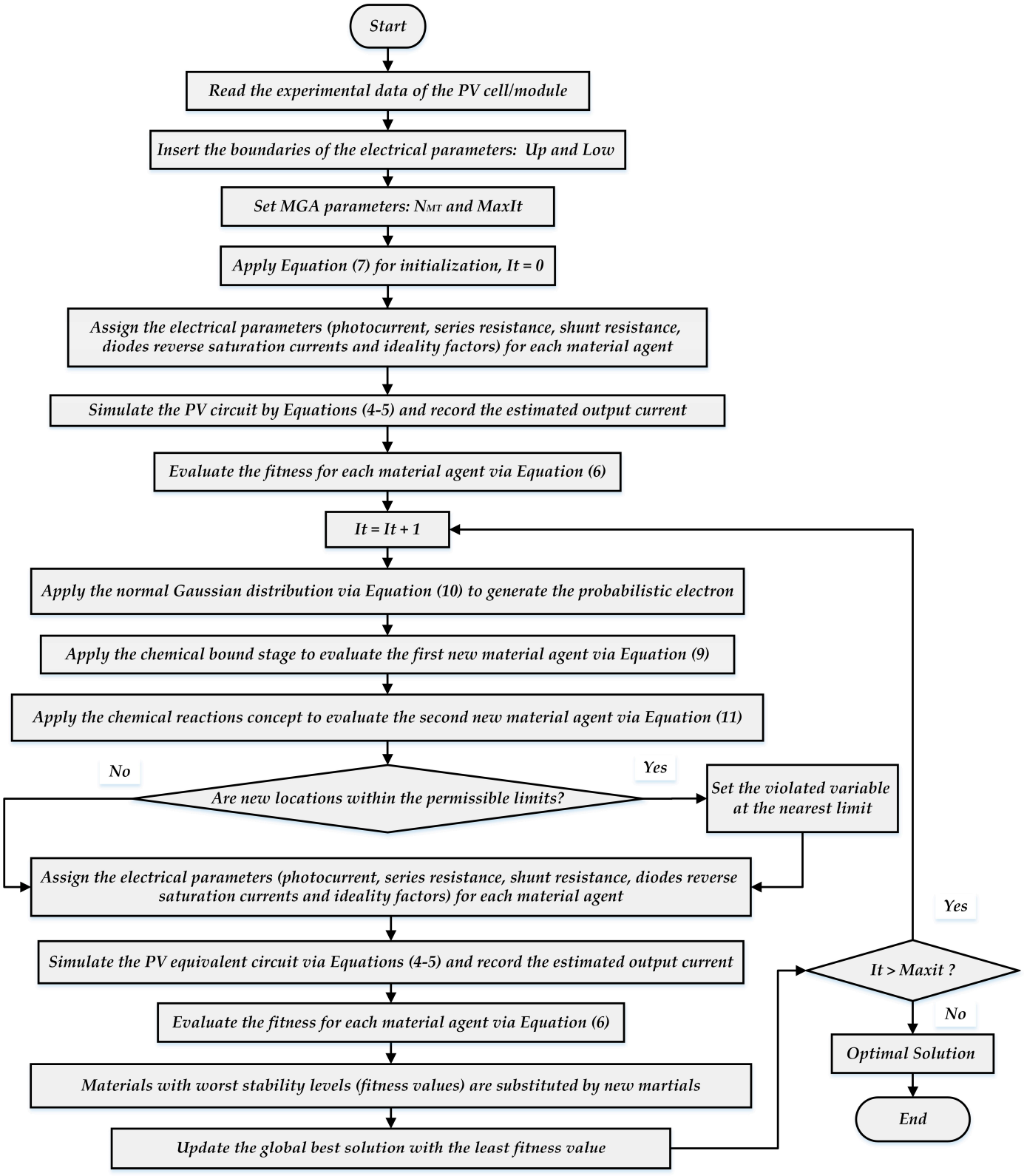


Figure 3. Main steps of MGA.

4. Simulation Results

This section examines R.T.C. France and the Kyocera KC200GT PV module using the recommended MGA methodology. The first case study focuses on a commercial silicon solar R.T.C. France module that has a sun radiance of 1000 W/m^2 and runs at 33 degrees Celsius. It has an open circuit voltage of 0.5727 V and a short-circuit current of 0.7605 A. Moreover, the maximum point voltage and current of R.T.C. France are 0.4590 V and 0.6755 A, respectively. The second case study concerns the Kyocera KC200GT PV Module, which has an open-circuit voltage of (32.90 V) and a short-circuit current of (8.21 A) and is made up of 54 multi-crystalline cells connected in series. The maximum power points, voltage, and current for this module are 200 W, 26.30 V, and 7.61 A, respectively. Table 1 displays the acquired characteristics of the RTC France and KC200GT PV modules along with their upper limit (UL) and lower limit (LL). This section examines and applies the MGA technique to parameter extraction problems for different solar cells/modules of the SD and DD models in order to compare it with other optimization strategies that have been somewhat well-reported. The same 1000 iterations and 200 people are used while applying MGA. Added to that, detailed specifications for both the RTC France PV cell and the Kyocera KC200GT PV module are displayed in Tabel 1.

Table 1. Limits of the PV cell parameters and technical specifications of RTC France cell and Kyocera KC200GT module.

Parameter	RTC France		Kyocera KC200GT	
	Low	Up	Low	Up
R_{ss} (Ω)	0	0.5	0	2
R_{sh} (Ω)	0	100	0	100
η_1 and η_2 per cell	1	2	1	2
I_{ph} (A)	0	1	0	10
I_{S1} and Is_2 (μA)	0	1	0	10
No series cells	1		54	
Maximum Power (Pmax)	33.15 W		200 W	
Open Circuit Voltage (Voc)	0.5727 V		32.90 V	
Short Circuit Current (Isc)	0.7605 A		8.21 A	
Voltage at Pmax (Vm)	0.4590 V		26.30 V	
Current at Pmax (Im)	0.6755 A		7.61 A	
Cell Area	2 cm^2		1.39 m^2	
Cell Technology	Monocrystalline Silicon		54 multicrystalline cells	
Operating Temperature	25 °C		25 °C	
Efficiency	~12–15%		16%	

4.1. Applications of RTC France PV

4.1.1. Case 1: SD Model of RTC France PV

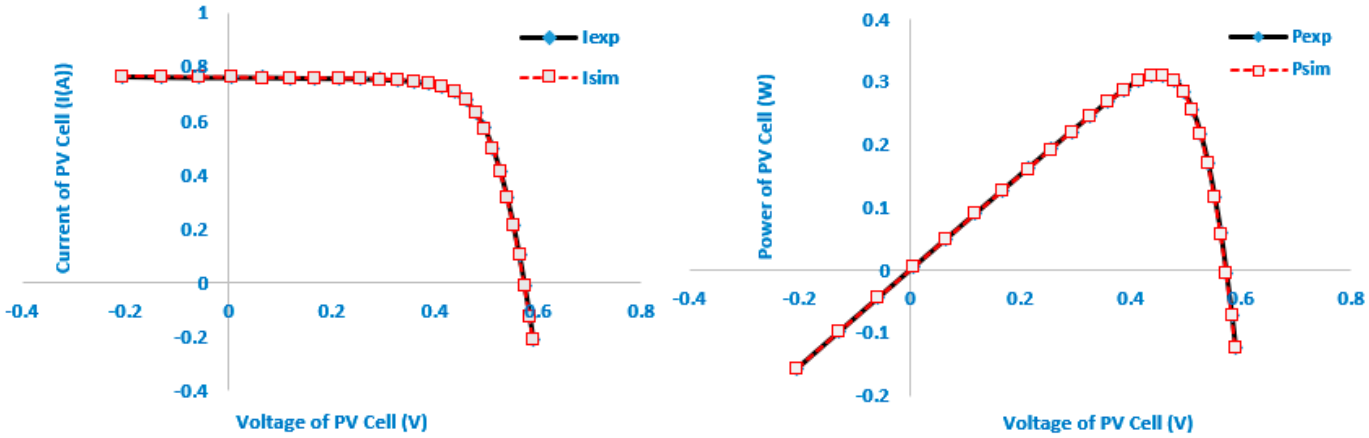
In this instance, the recommended MGA is used to extract the R.T.C. France cell's SD model features. The five unknown SD model parameters for various inspirational approaches that produced the greatest results in the experiment are listed in Table 2. The findings demonstrate that, in terms of competitiveness, the suggested MGA performs better than the comparable methods. This indicates that the optimal RMSE value of 9.8249×10^{-4} is achieved by the suggested MGA. Furthermore, the table shows the PV-derived electrical parameters using the established optimization techniques; these include the HEAP Optimizer [44], Barnacles Mating Optimizer (BMA) [45], Lightning Attachment Procedure Optimization (LAPO) [46], Classified perturbation mutation PSO (CPMPSO) [47],

hybrid PSO–GWO algorithm (PSOGWO) [48], RIME [49], a performance-guided JAYA (PGJAYA) [50], Enhanced MPA (EMPA) [44], neighborhood scheme-based Laplacian MBA (NLBMA) [51], Equilibrium Optimizer (EO) [44], multi-verse optimizer (MVO) [52], Enriched Harris Hawks optimization (EHHO) [53], particle swarm optimization (PSO) [54], Ant Lion Optimizer (ALO) [55], Growth optimizer GO [56], Jellyfish Search (JFS) Optimizer [44], flexible PSO (FPSO) [20], Hybrid Firefly and Pattern Search (HFAPS) [57], and Marine Predator Algorithm (MPA) [44]. Moreover, the table specifies the assessed parameters of the proposed MGA, which are 53.71852 Ω, 0.036377 Ω, 0.760776 A, 3.23×10^{-1} µA, and 1.481184 for the shunt resistance, series resistance, photo-current, saturation current for d1, and ideality factor for d1, respectively.

Table 2. Acquired parameters for the R.T.C. France PV module (SD model) using MGA compared to the reported results.

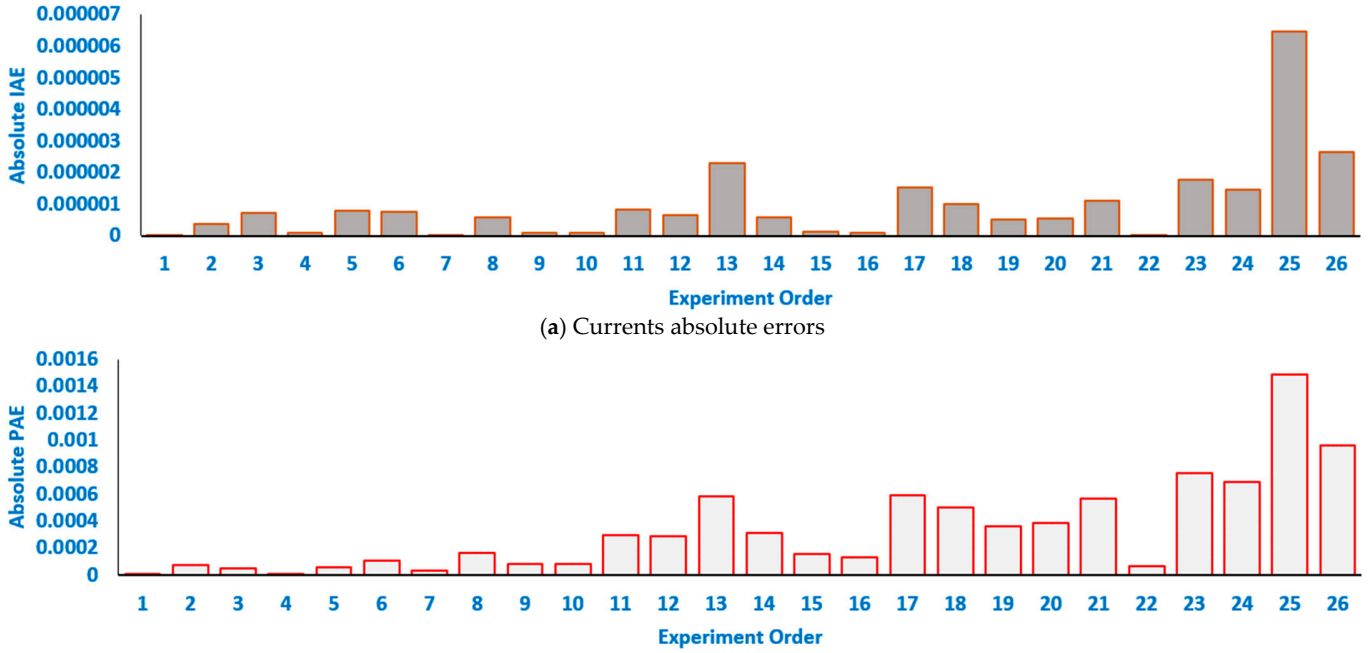
Algorithm	I_{ph} (A)	I_{sd} (µA)	n	R_{sh} (Ω)	R_{ss} (Ω)	*RMSE*
MGA	0.760776	3.23×10^{-1}	1.481184	53.71852	0.036377	9.8602×10^{-4}
RIME [49]	0.760776	3.23021×10^{-1}	1.481184	53.71865291	0.036377096	9.9755×10^{-4}
PGJAYA [50]	8.2167	0.002284	58.1742	773.8117	0.3435	1.5455×10^{-4}
MPA [44]	8.184927	7.94459×10^{-2}	1.285180059	92.14823504	0.004537611	1.487×10^{-2}
JFS [44]	8.193182	4.72×10^{-2}	1.250052	14.97462	0.004679	9.477×10^{-3}
GO [56]	8.192967	4.31808×10^{-2}	1.244346	15.103921	0.004710	8.515347×10^{-3}
HFAPS [57]	8.1992	0.154161	74.5795	1448.2590	0.2396	4.9863×10^{-2}
CPMPSO [47]	8.21689146	0.00224195	1.07641028	763.535149	0.34381405	1.53903×10^{-3}
EHHO [53]	8.2224	0.000001	80.6915	1806.0252	0.1835	5.9507×10^{-2}
FPSO [20]	8.2186	0.001436	56.9854	130.2813	0.2409	2.8214×10^{-2}
PSOGWO [48]	8.2132	9.6768	1.7463	38.8968	0.0011	1.2700×10^{-1}
EO [44]	8.209153	2.85×10^{-2}	1.218068	7.714703	0.004815	2.888×10^{-3}
PSO [54]	8.2027	2.8852	1.6052	33.8855	0.0019	1.0195×10^{-1}
MVO [52]	8.2527	0.063908	69.2388	134.4813	0.1341	8.3800×10^{-2}
BMA [45]	8.1950	3.1015	1.6130	100.0000	0.0019	1.0244×10^{-1}
LAPO [46]	8.2155	8.1491	1.7258	5.0000	0.001	1.3813×10^{-1}
EMPA [44]	8.21195	3.59×10^{-2}	1.232551	7.560713	0.004742	3.847×10^{-3}
NLBMA [51]	8.1467	0.0022	1.0839	5.0000	0.0045	3.3610×10^{-2}
HEAP [44]	8.200974	4.49×10^{-2}	1.246924	11.87468	0.004696	7.425×10^{-3}

Figure 4a,b displays the measured and simulated I–V and P–V characteristics for the SD model. It is observable that the data produced by the suggested MGA technique closely resemble the data acquired by experimentation, suggesting that the MGA technique was successful in producing power and current at a range of voltage levels. The simulation and measured current absolute errors range from 6.65894×10^{-9} to 6.4686×10^{-6}, while the simulation and measured power absolute errors range from 1.85822×10^{-6} to 1.4835×10^{-3}, as shown in Figure 5a,b.



(**a**) (**b**)

Figure 4. (**a**) I–V and (**b**) P–V characteristics for the SD of the R.T.C. France cell using the suggested MGA.



(**a**) Currents absolute errors

(**b**) Powers absolute errors

Figure 5. Overall discrepancies in currents and powers between the measured and simulated for the SD model of the R.T.C. France cell using MGA.

4.1.2. Case 2: DD Model of RTC France PV

In this instance, the recommended MGA is used to extract the R.T.C. France cell's DD model features. The seven unknown DD model parameters for various inspirational approaches that produced the greatest results in the experiment are listed in Table 3. The findings demonstrate that, in terms of competitiveness, the suggested MGA performs better than the comparable methods. This indicates that the optimal RMSE value of 9.8249×10^{-4} is achieved by the suggested MGA. Furthermore, this Table shows the PV-derived electrical parameters using the established optimization techniques; these include the Dwarf Mongoose Optimizer (DMO) [58], RIME [49], modified DMO [58], and modified RIME [49]. Moreover, this Table specifies the assessed parameters of the proposed MGA, which are 55.485441 Ω, 0.0367404 Ω, 0.7607811 A, 7.493×10^{-1} μA, 2.26×10^{-1} μA, and 2, 1.4510 for the shunt resistance, series resistance, photo-current, saturation current for d1 and d2, and ideality factor for d1 and d2 respectively.

Table 3. Acquired parameters for the R.T.C. France PV module (DD model) using MGA compared to the reported results.

Applied Algorithm	RIME	DMO	MRIME	MDMO	MGA
I_{Ph} (A)	0.760864277	0.761086003	0.760780758	0.760777046	0.760781079
R_{ss} (Ω)	0.036173672	0.036452844	0.036767981	0.03658083	0.03674043
R_{Sh} (Ω)	53.58354831	56.0407128	55.64800559	54.7047585	55.48544096
I_{S1} (A)	4.3113×10^{-8}	3.81141×10^{-7}	8.0438×10^{-7}	4.27843×10^{-7}	7.49347×10^{-7}
η_1	1.827202939	1.83357911	1.999974446	1.991913976	2
I_{S2} (A)	3.25421×10^{-7}	2.38858×10^{-7}	2.19744×10^{-7}	2.63353×10^{-7}	2.25974×10^{-7}
η_2	1.482783518	1.458364626	1.448694376	1.463888853	1.45101678
RMSE	9.9382×10^{-4}	1.028696×10^{-3}	9.8251×10^{-4}	9.83217×10^{-4}	9.82485×10^{-4}

Furthermore, Figure 6 illustrates fifty obtained RMSE objectives for the SD and DD of the R.T.C. France cell. This figure characterizes that the RMSE of MGA for the SD and DD models are 9.86022×10^{-4} and 9.82485×10^{-4}. The worst values for the SD and DD models are the same value of 9.86022×10^{-4}. The mean values for the SD and DD models are 9.86022×10^{-4} and 9.83096×10^{-4}, respectively. The standard deviation for the SD and DD models are 1.49963×10^{-17} and 1.29387×10^{-6}, respectively. These outcomes support the developed MGA's superiority for the R.T.C. France cell's SD and DD models. As a result, the recommended MGA produced the most significant value, showing that MGA ensures stability, precision, and effectiveness when comparing the parameters of the SD and DD models. The MGA's identification of the SD and DD models' validity is dependable.

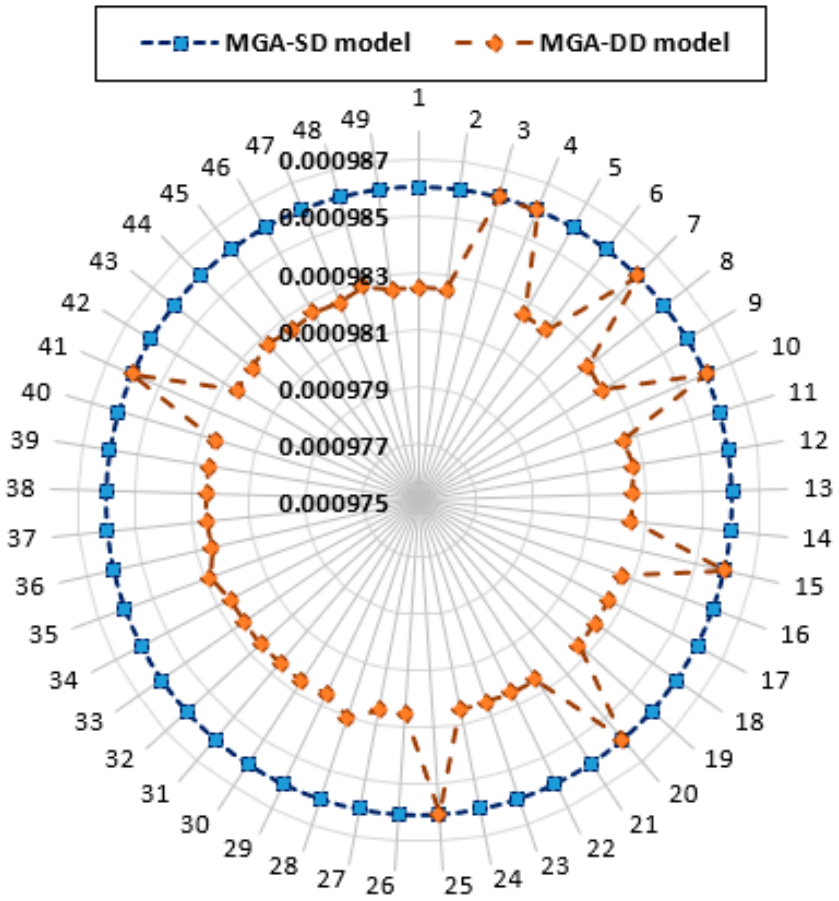
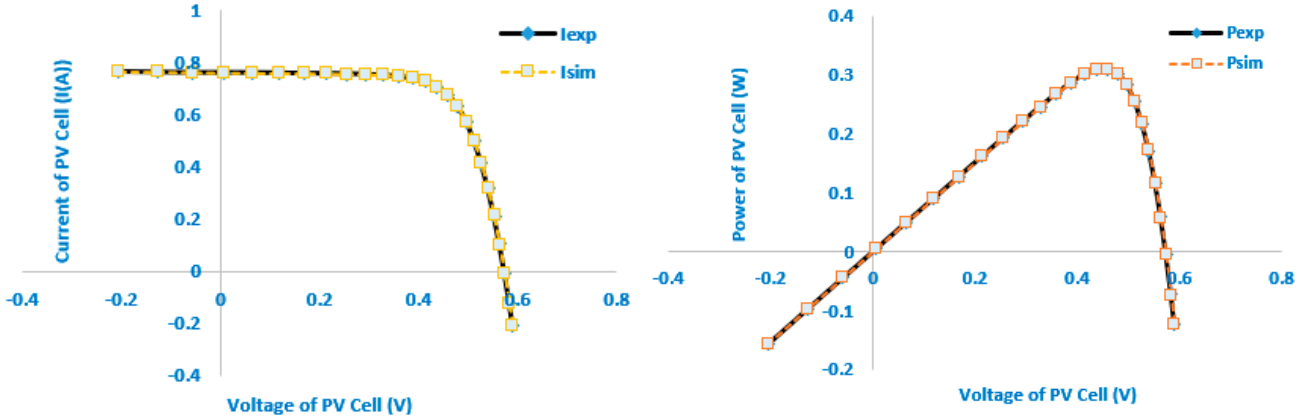


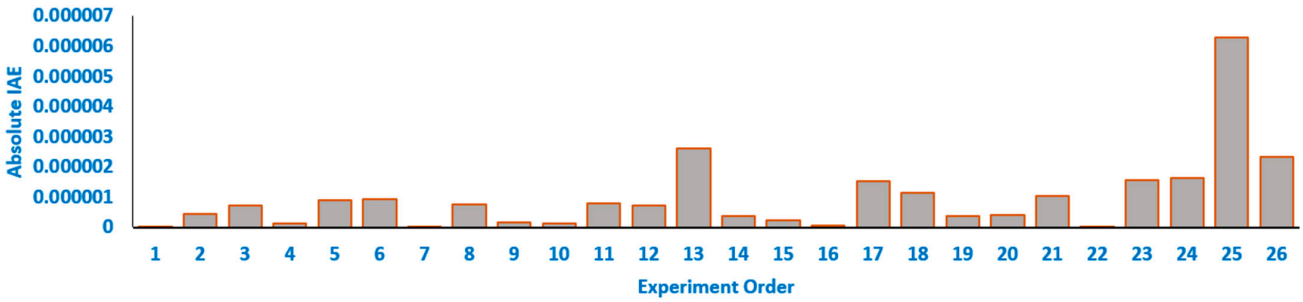
Figure 6. Fifty obtained RMSE objectives for SD and DD models of the R.T.C. France cell.

Figure 7a,b display the measured and simulated I–V and P–V characteristics for the DD model. It is demonstrable that the data generated by the MGA technique closely resemble the data acquired by experimentation, suggesting that the MGA technique was successful in producing power and current at a range of voltage levels. Figure 8a,b illustrate that the simulated and measured current absolute errors range from 7.69197×10^{-9} to 6.28712×10^{-6}, while the simulated and measured power absolute errors range from 1.97225×10^{-6} to 1.4626×10^{-3}.

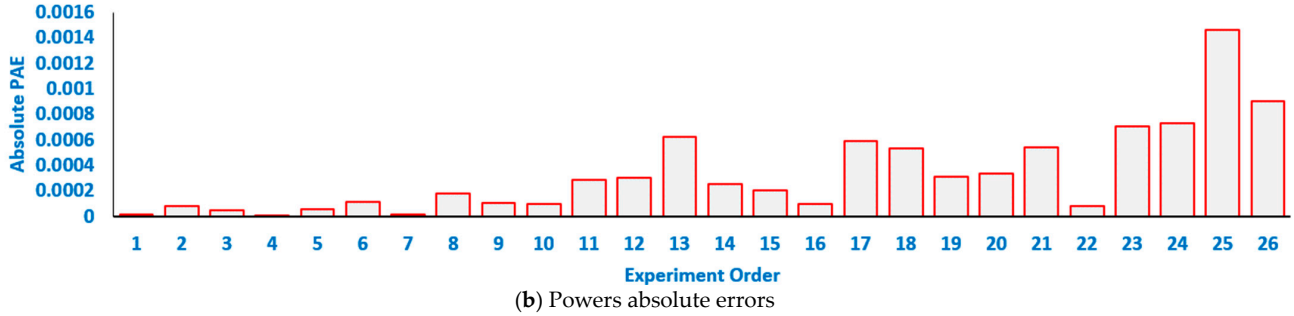


(**a**) (**b**)

Figure 7. (**a**) I–V and (**b**) P–V characteristics for the DD of the R.T.C. France cell using the suggested MGA.



(**a**) Currents absolute errors



(**b**) Powers absolute errors

Figure 8. Overall discrepancies in currents and powers between the measured and simulated for the DD model of the R.T.C. France cell using MGA.

4.2. Applications of KC200GT PV Module

4.2.1. Case 1: SD Model of KC200GT PV Module

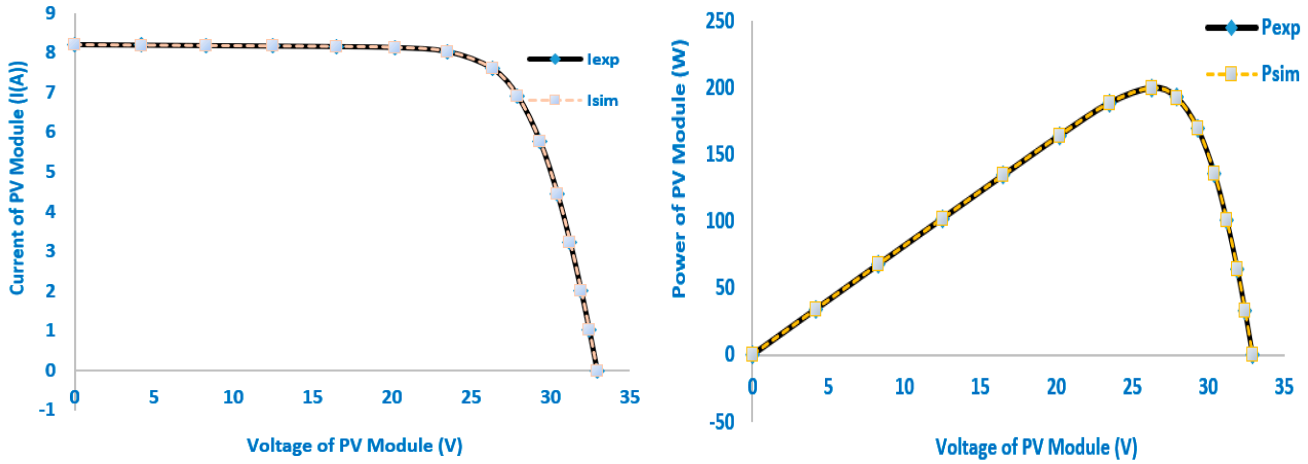
In this instance, the recommended MGA is used to extract the KC200GT PV module's SD model features. The five unknown SD model parameters for various inspirational approaches that produced the greatest results in the experiment are listed in Table 4. The findings demonstrate that, in terms of competitiveness, the suggested MGA performs better than the comparable methods. This indicates that the optimal RMSE value of

7.548013×10^{-3} is achieved by the suggested MGA. Furthermore, the table shows the PV-derived electrical parameters using the established optimization techniques; these include the Growth optimizer (GO) [56], energy valley optimizer (EVO) [56], and Hazelnut tree search (HTS) algorithm [56].

Table 4. Acquired parameters for the KC200GT PV module (the SD model) using MGA compared to others.

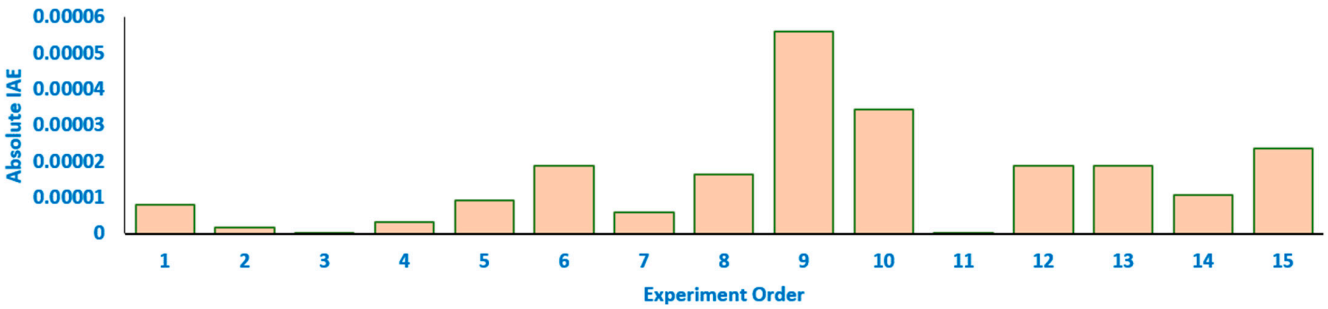
Applied Technique	HTS	EVO	GO	MGA
I_{ph} (A)	8.190356368	8.214036069	8.192967279	8.206335844
R_{sh} (Ω)	53.11148143	13.69688319	15.10392113	9.197019679
R_S (Ω)	0.004417871	0.00428964	0.004709892	0.004659152
I_{S1} (A)	1.12138×10^{-7}	1.42038×10^{-7}	4.31808×10^{-8}	4.81328×10^{-8}
η_1	1.309576425	1.326768155	1.244345573	1.251560118
RMSE	0.01799763	0.023069893	0.008515347	0.007548013

Figure 9a,b display the measured and simulated I–V and P–V characteristics for the SD model. It is observable that the data produced by the suggested MGA technique closely resemble the data acquired by experimentation, suggesting that the MGA technique was successful in producing power and current at a range of voltage levels. The simulation and measured current absolute errors range from 1.26882×10^{-8} to 5.61013×10^{-5}, while the simulation and measured power absolute errors range from 0 to 2.0897×10^{-1}, as shown in Figure 10a,b.



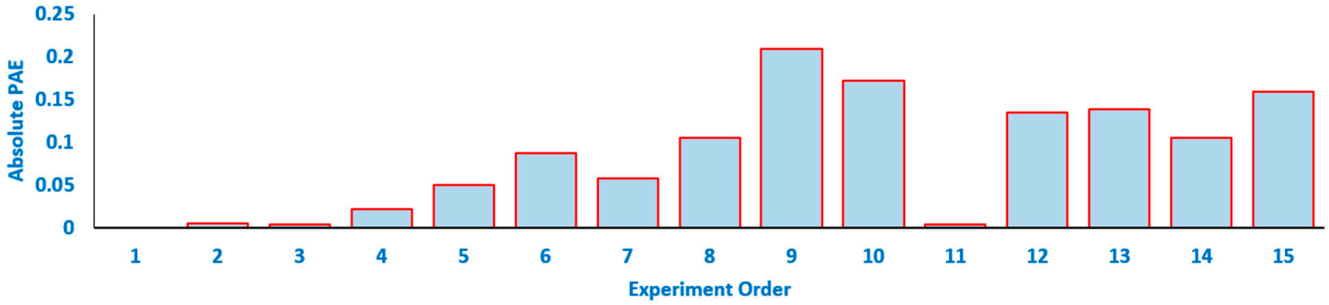
(**a**) (**b**)

Figure 9. (**a**) I–V and (**b**) P–V characteristics for the SD of the KC200GT PV module using the suggested MGA.



(**a**) Currents absolute errors

Figure 10. *Cont.*



(**b**) Powers absolute errors

Figure 10. Overall discrepancies in currents and powers between the measured and simulated for the SD model of the KC200GT PV module using MGA.

4.2.2. Case 2: DD Model of KC200GT PV Module

In this instance, the recommended MGA is used to extract the KC200GT PV module's DD model features. The seven unknown SD model parameters for various inspirational approaches that produced the greatest results in the experiment are listed in Table 5. The findings demonstrate that, in terms of competitiveness, the suggested MGA performs better than the comparable methods. This indicates that the optimal RMSE value of 5.91445×10^{-4} is achieved by the suggested MGA. Furthermore, the table shows the PV-derived electrical parameters using the established optimization techniques; these include the HTS, GO, and EVO.

Table 5. Acquired parameters for the KC200GT PV module (the DD model) using MGA compared to others.

Applied Technique	HTS	EVO	GO	MGA
I_{ph} (A)	8.203823597	8.20424482	8.193643057	8.216682898
R_{sh} (Ω)	92.46395147	66.83697866	16.37828656	6.303160786
R_S (Ω)	0.004562321	0.004219395	0.004688805	0.004829466
I_{S1} (A)	5.66339×10^{-8}	1.82124×10^{-7}	6.01244×10^{-8}	8.65143×10^{-9}
η_1	1.749082759	1.346598774	1.832451271	1.315186385
I_{S2} (A)	8.0133×10^{-8}	5.75716×10^{-7}	4.57891×10^{-8}	2.12348×10^{-8}
η_2	1.286121414	1.933055486	1.248347215	1.20450769
RMSE	0.020515491	0.02717656	0.009049475	0.000591445

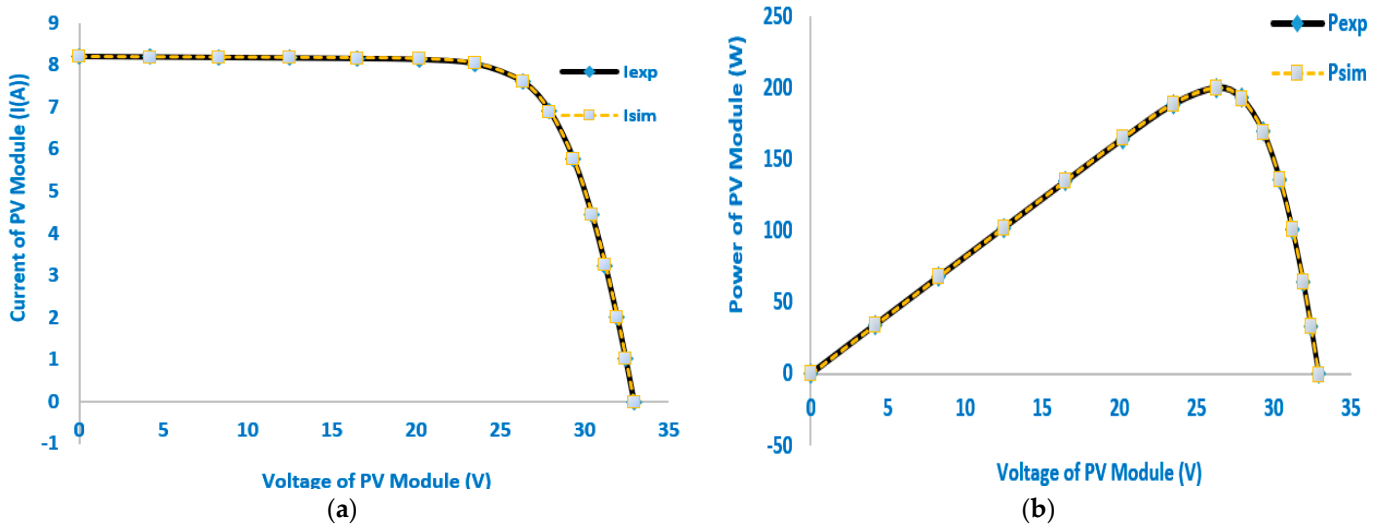
Figure 11a,b display the measured and simulated I–V and P–V characteristics for the SD model. It is observable that the data produced by the suggested MGA technique closely resemble the data acquired by experimentation, suggesting that the MGA technique was successful in producing power and current at a range of voltage levels. The simulation and measured current absolute errors range from 3.74212×10^{-7} to 3.45977×10^{-4}, while the simulation and measured power absolute errors range from 0 to 6.1195×10^{-1}, as shown in Table 6.

Table 6. Absolute errors in currents and powers between the measured and simulated for the DD model of the KC200GT PV module using MGA.

MGA	Vexp	Iexp	Isim	Pexp	Psim	Absolut IAE	Absolut PAE
1	0	8.21	8.197656	0	0	0.000152365	0
2	4.2	8.198	8.191457	34.4316	34.40412	4.28089×10^{-5}	0.027479989
3	8.3	8.186	8.185388	67.9438	67.93872	3.74212×10^{-7}	0.005077348

Table 6. *Cont.*

MGA	Vexp	Iexp	Isim	Pexp	Psim	Absolut IAE	Absolut PAE
4	12.5	8.174	8.17898	102.175	102.2373	2.48013×10^{-5}	0.062251164
5	16.5	8.161	8.171047	134.6565	134.8223	0.000100951	0.165782965
6	20.2	8.136	8.149286	164.3472	164.6156	0.000176507	0.268368678
7	23.5	8.035	8.042986	188.8225	189.0102	6.37699×10^{-5}	0.187661708
8	26.3	7.61	7.601657	200.143	199.9236	6.95992×10^{-5}	0.219410741
9	27.9	6.915	6.899606	192.9285	192.499	0.000236968	0.429486287
10	29.3	5.785	5.775501	169.5005	169.2222	9.02342×10^{-5}	0.278325669
11	30.4	4.458	4.461943	135.5232	135.6431	1.55451×10^{-5}	0.119858843
12	31.2	3.239	3.250869	101.0568	101.4271	0.000140875	0.370314599
13	31.9	2.006	2.015922	63.9914	64.30792	9.84526×10^{-5}	0.316522341
14	32.4	1.036	1.038177	33.5664	33.63693	4.73849×10^{-6}	0.070528555
15	32.9	0	−0.0186	0	−0.61195	0.000345977	0.611954698



(**a**) (**b**)

Figure 11. (**a**) I–V and (**b**) P–V characteristics for the DD of the KC200GT PV module using the suggested MGA.

4.2.3. Case 3: The Effect of Varying the Weather on SD and DD Models

The performance of PV systems is significantly affected by environmental factors such as irradiation and temperature, as well as aging, dust, and pollutants. These elements affect the power output by reducing the cell's efficiency, causing deviations in the expected performance under normal conditions. Specifically, irradiation and temperature significantly impact the performance of PV systems. Higher irradiation increases the current generation, improving power output, while lower irradiation reduces it. However, temperature has an inverse effect; as temperatures rise, the voltage decreases, leading to a reduction in overall efficiency. The combined effects of high irradiation and temperature often result in a trade-off where power gains from increased sunlight are offset by thermal losses. Added to that, as PV cells age, their efficiency gradually decreases due to wear and tear of materials, resulting in lower current and voltage output. Also, the accumulation of dust and pollutants on the surface of PV modules reduces the amount of sunlight reaching the cells, limiting the energy conversion efficiency. This leads to a mismatch between the expected and actual performance. These environmental factors can result in inaccurate modeling if not accounted for, leading to deviations between simulated and actual PV performance.

To handle these impacts on PV cell performance, the proposed MGA simulates various operational conditions by incorporating real-time data across different environmental scenarios. Specifically, the MGA adjusts parameter values dynamically to account for varying irradiance and temperature levels. The efficiency of PV modules fluctuates depending on irradiation levels and temperature. In the study, the MGA's effectiveness was evaluated using five different irradiances (200 W/m^2, 400 W/m^2, 600 W/m^2, 800 W/m^2, and 1000 W/m^2), with the temperature held constant at 25 °C. Additionally, experiments were conducted at a fixed irradiance of 1000 W/m^2 with varying temperatures of 25 °C, 50 °C, and 75 °C.

Additionally, the efficiency of the suggested MGA approach is verified in comparison to GO, EVO, and HTS in a range of meteorological scenarios. The data were gathered using five different irradiances: 200 W/m^2, 400 W/m^2, 600 W/m^2, 800 W/m^2, and 1000 W/m^2. The temperature was kept constant at 25 °C. Furthermore, with a fixed irradiance of 1000 W/m^2, the KC200GT can be obtained in three temperatures: 25 °C, 50 °C, and 75 °C. The results of the optimal parameters obtained by the proposed MGA for the SD and DD models are presented in Tables 7 and 8, along with a comparison with the reported methodologies, including the EVO, GO, HTS, and FPA approaches. The better performance of the suggested GO approach is seen for all the weather scenarios examined for the SD and DD models.

Table 7. Acquired parameters for the KC200GT PV module of the SD model under various weather scenarios using MGA compared to others.

(a) Irradiance of 200 W/m^2 at temperature of 25 °C					
Applied technique	GO	FPA	EVO	HTS	MGA
I_{Ph} (A)	1.641655	1.641477	1.614391	1.63522	1.642501
R_{sh} (Ω)	6.661734	6.679449	55.9507	8.863031	6.599083
I_{S1} (A)	2.22×10^{-8}	1.96×10^{-8}	4.13×10^{-7}	1.33×10^{-7}	3.03×10^{-8}
R_S (Ω)	0.004559	0.004758	0.000533	0.001718	0.004049
η_1	1.223433	1.215165	1.456835	1.357627	1.245026
RMSE	0.000955	0.001513	0.013567	0.004668	0.000679
(b) Irradiance of 400 W/m^2 at temperature of 25 °C					
Applied technique	GO	FPA	EVO	HTS	MGA
I_{Ph} (A)	3.277192	3.28093	3.258167	3.276746	3.283439
R_{sh} (Ω)	8.306541	8.180287	28.1826	10.69592	7.09384
I_{S1} (A)	3.70×10^{-8}	4.63×10^{-8}	6.40×10^{-8}	1.14×10^{-7}	4.13×10^{-8}
R_S (Ω)	0.004447	0.004235	0.004266	0.003628	0.004338
η_1	1.247147	1.262536	1.285174	1.32855	1.254853
RMSE	0.003933	0.0048	0.012554	0.007983	0.002569
(c) Irradiance of 600 W/m^2 at temperature of 25 °C					
Applied technique	GO	FPA	EVO	HTS	MGA
I_{Ph} (A)	4.918437	4.908892	4.911306	4.906687	4.926221
R_{sh} (Ω)	8.889982	14.51855	12.05364	22.41087	7.464378
I_{S1} (A)	3.51×10^{-8}	5.43×10^{-8}	2.32×10^{-8}	1.60×10^{-7}	4.57×10^{-8}
R_S (Ω)	0.004639	0.004507	0.004805	0.003882	0.004523
η_1	1.237893	1.266975	1.210601	1.34608	1.255605
RMSE	0.00588	0.009391	0.01287	0.014001	0.004463

Table 7. *Cont.*

(d) Irradiance of 800 W/m^2 at temperature of 25 °C					
Applied technique	GO	FPA	EVO	HTS	MGA
I_{Ph} (A)	8.441114	8.441114	8.320163	8.410788	6.570051
R_{sh} (Ω)	1.602797	1.602796	11.25177	2.046745	7.485995
I_{S1} (A)	0.000001	1.00×10^{-6}	0.000001	1.00×10^{-6}	4.24×10^{-8}
R_S (Ω)	0.005628	0.005628	0.005796	0.005674	0.004646
η_1	1.212172	1.212172	1.211071	1.211876	1.246328
RMSE	0.039212	0.039212	0.058525	0.040739	0.005127
(e) Irradiance of 1000 W/m^2 at temperature of 50 °C					
Applied technique	GO	FPA	EVO	HTS	MGA
I_{Ph} (A)	8.301133	8.298574	8.266066	8.296297	8.301133
R_{sh} (Ω)	5.62421	6.134123	33.15247	6.661412	5.624207
I_{S1} (A)	6.15×10^{-7}	6.83×10^{-7}	8.91×10^{-7}	7.23×10^{-7}	6.15×10^{-7}
R_S (Ω)	0.00484	0.004803	0.004752	0.00479	0.00484
η_1	1.310146	1.318481	1.339864	1.323004	1.208789
RMSE	0.001562	0.002195	0.011639	0.002984	0.001562
(f) Irradiance of 1000 W/m^2 at temperature of 75 °C					
Applied technique	GO	FPA	EVO	HTS	MGA
I_{Ph} (A)	8.441114	8.441114	8.320163	8.410788	8.441114
R_{sh} (Ω)	1.602797	1.602796	11.25177	2.046745	1.602796
I_{S1} (A)	0.000001	1.00×10^{-6}	0.000001	1.00×10^{-6}	1×10^{-6}
R_S (Ω)	0.005628	0.005628	0.005796	0.005674	0.005628
η_1	1.212172	1.212172	1.211071	1.211876	1.038085
RMSE	0.039212	0.039212	0.058525	0.040739	0.039212

At irradiance of 200 W/m^2 at temperature of 25 °C, for the SD model, the MGA shows a 28.901% improvement in reducing the RMSE compared to the closest algorithm. For the DD model, the improvement is even more significant, with an 8.07% reduction in RMSE compared to the closest algorithm. At irradiance of 400 W/m^2 and a temperature of 25 °C, the MGA optimizer demonstrates a 34.681% improvement in RMSE for the SD model compared to the closest algorithm. However, for the DD model, the improvement is notably higher at 90.29%. At irradiance of 600 W/m^2 at temperature of 25 °C, the MGA optimizer shows a 24.099% improvement for the SD model and a 14.53% improvement for the DD model in reducing RMSE, compared to the closest algorithm. At an irradiance of 800 W/m^2 and a temperature of 25 °C, the MGA optimizer demonstrates a significant 86.925% improvement for the SD model and a 62.89% improvement for the DD model in reducing RMSE compared to the closest algorithm. These results suggest that the MGA optimizer excels in capturing the parameters accurately under high irradiance levels.

The proposed MGA approach produced low RMSE values at various temperatures and irradiances, as shown in Figures 12 and 13. To gain a better understanding of the proposed MGA technique's capacity to determine unidentified PV parameters, Figure 14a displays the I–V data modeled by the technique at different temperatures with respect to 1000 W/m^2 irradiance, and Figure 14b shows the same data at 25 °C with respect to different irradiance. (b). The P–V data simulated by the suggested MGA technique at various temperatures—1000 W/m^2 irradiance at 25 °C and variable irradiance at other temperatures—are displayed in Figure 15a,b. The I–V and P–V data sheets from the

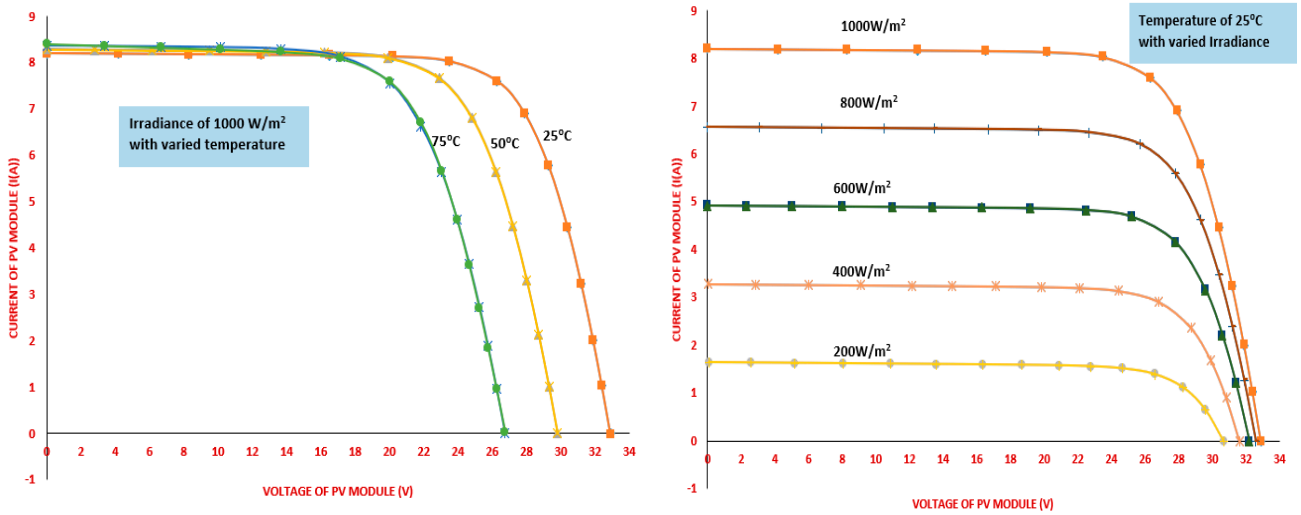
manufacturer have been adapted to those simulated curves. When it comes to determining the PV parameters at different temperatures and irradiance, the recommended MGA technique performs better than commercial PV systems. This indicates the efficacy of the suggested methodology and its capacity to produce highly consistent fitted I–V data with manufacturers' data sheets.

Table 8. Acquired parameters for the KC200GT PV module of the DD model under various weather scenarios using MGA compared to others.

(a) Irradiance of 200 W/m^2 at temperature of 25 °C					
Applied technique	GO	EVO	HTS	FPA	MGA
I_{Ph} (A)	1.641698	1.623979	1.642334	1.645062	1.642894
R_{sh} (Ω)	6.745461	20.39073	6.904484	6.167409	6.578741
I_{S1} (A)	8.37×10^{-8}	2.16×10^{-7}	1.02×10^{-7}	0	0
η_1	1.953584	2	1.336849	1.835084	1.95091
I_{S2} (A)	3.10×10^{-8}	5.38×10^{-7}	9.80×10^{-8}	2.75×10^{-8}	3.27×10^{-8}
$H2$	1.246916	1.484407	1.890871	1.238244	1.250303
R_S (Ω)	0.003971	1.01×10^{-19}	0.00172	0.004099	0.003932
RMSE	0.000917	0.011151	0.003912	0.001825	0.000843
(b) Irradiance of 400 W/m^2 at temperature of 25 °C					
Applied technique	GO	EVO	HTS	FPA	MGA
I_{Ph} (A)	3.281489	3.26987	3.276352	3.277503	3.286687
R_{sh} (Ω)	7.399506	16.74248	10.39877	8.571691	6.411204
I_{S1} (A)	1.85×10^{-8}	1.21×10^{-7}	4.02×10^{-7}	0	6.12×10^{-9}
$\eta 1$	1.204604	1.844696	2	2	1.162323
I_{S2} (A)	5.72×10^{-7}	3.65×10^{-7}	1.77×10^{-7}	6.30×10^{-8}	3.14×10^{-8}
$H2$	1.838341	1.425606	1.364486	1.284554	1.307248
R_S (Ω)	0.004712	0.002429	0.003023	0.004064	0.004811
RMSE	0.001997	0.013536	0.010082	0.005031	0.000194
(c) Irradiance of 600 W/m^2 at temperature of 25 °C					
Applied technique	GO	EVO	HTS	FPA	MGA
I_{Ph} (A)	4.919192	4.904594	4.924728	4.91092	4.923462
R_{sh} (Ω)	9.116196	27.02803	12.86054	12.76529	7.941242
I_{S1} (A)	4.81×10^{-8}	6.61×10^{-8}	8.48×10^{-8}	6.99×10^{-8}	4.75×10^{-8}
$\eta 1$	1.259016	1.28209	1.300237	1.284889	1.258202
I_{S2} (A)	9.19×10^{-9}	5.46×10^{-7}	1.67×10^{-7}	4.58×10^{-8}	1.42×10^{-8}
$H2$	1.698114	1.903013	1.728064	1.967746	1.892401
R_S (Ω)	0.00449	0.004365	0.004266	0.004341	0.004497
RMSE	0.005683	0.012289	0.013487	0.009196	0.004857
(d) Irradiance of 800 W/m^2 at temperature of 25 °C					
Applied technique	GO	EVO	HTS	FPA	MGA
I_{Ph} (A)	8.423041	8.311589	8.358966	8.423242	6.560835
R_{sh} (Ω)	1.993537	7.206907	4.84717	1.992924	13.05214
I_{S1} (A)	1.00×10^{-6}	6.71×10^{-7}	0.000001	0.000001	0
$\eta 1$	1.266804	1.223431	1.265694	1.265644	1.28582

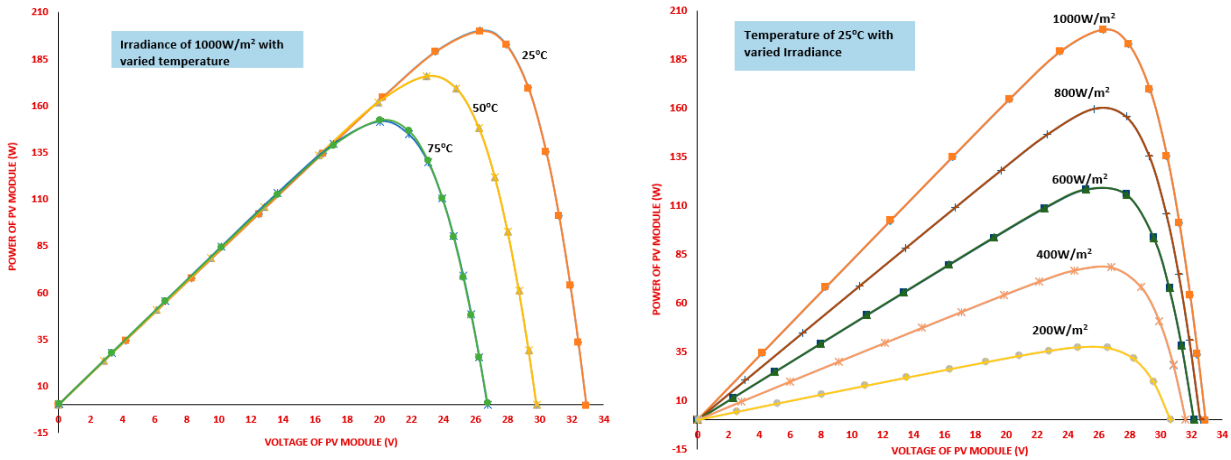
Table 8. *Cont.*

(d) Irradiance of 800 W/m^2 at temperature of 25 °C					
Applied technique	GO	EVO	HTS	FPA	MGA
I_{S2} (A)	1.00×10^{-6}	4.26×10^{-7}	0.000001	1.00×10^{-6}	7.18×10^{-8}
$H2$	1.266877	1.210971	1.266909	1.268029	1.281869
R_S (Ω)	0.005411	0.005719	0.005527	0.005411	0.004455
RMSE	0.029191	0.055535	0.037941	0.029195	0.010833
(e) Irradiance of 1000 W/m^2 at temperature of 50 °C					
Applied technique	GO	EVO	HTS	FPA	MGA
I_{Ph} (A)	8.300973	8.273769	8.285531	8.298369	8.301133
R_{sh} (Ω)	5.643489	20.07308	10.45826	6.19124	5.624185
I_{S1} (A)	5.03×10^{-9}	9.90×10^{-7}	7.66×10^{-7}	6.72×10^{-7}	6.15×10^{-7}
$\eta 1$	1.700812	1.754878	1.757351	1.317407	1.208789
I_{S2} (A)	6.14×10^{-7}	6.76×10^{-7}	7.61×10^{-7}	2.27×10^{-7}	1.25×10^{-15}
$H2$	1.310004	1.319326	1.328574	1.822645	1.000148
R_S (Ω)	0.004841	0.004803	0.004766	0.0048	0.00484
RMSE	0.001564	0.009872	0.00667	0.002403	0.001562
(f) Irradiance of 1000 W/m^2 at temperature of 75 °C					
Applied technique	GO	EVO	HTS	FPA	MGA
I_{Ph} (A)	8.423041	8.311589	8.358966	8.423242	8.424172
R_{sh} (Ω)	1.993537	7.206907	4.84717	1.992924	1.970199
I_{S1} (A)	1.00×10^{-6}	6.71×10^{-7}	0.000001	0.000001	0.000001
$\eta 1$	1.266804	1.223431	1.265694	1.265644	1.257094
I_{S2} (A)	1.00×10^{-6}	4.26×10^{-7}	0.000001	1.00×10^{-6}	9.93×10^{-7}
$H2$	1.266877	1.210971	1.266909	1.268029	1.277537
R_S (Ω)	0.005411	0.005719	0.005527	0.005411	0.005414
RMSE	0.029191	0.055535	0.037941	0.029195	0.029331



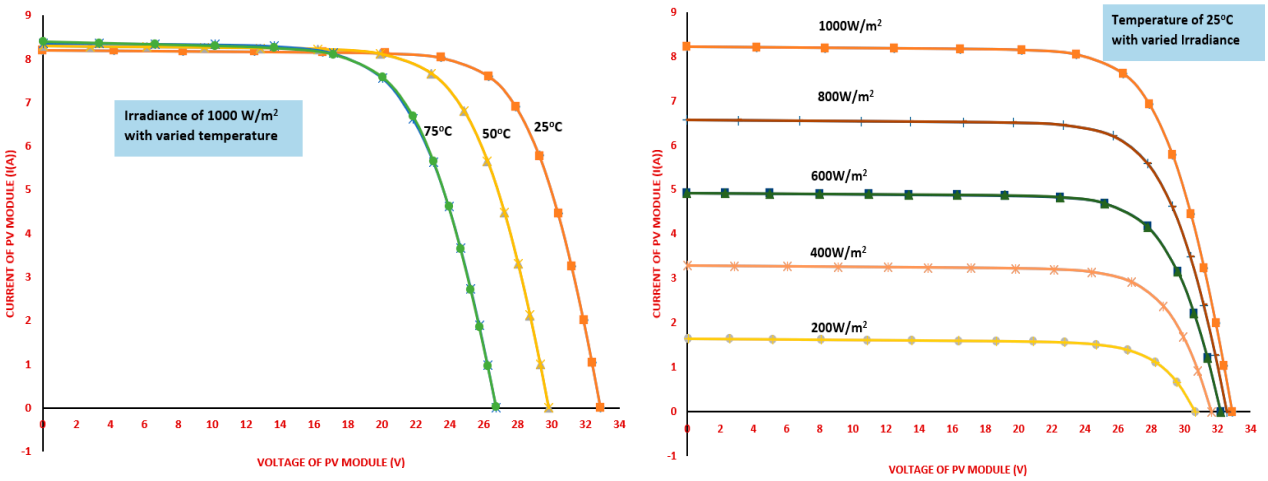
(**a**) **Varied Temperature** (**b**) Varied Irradiances

Figure 12. Acquired I–V characteristics for SD model of KC200GT PV module under various weather scenarios using MGA.



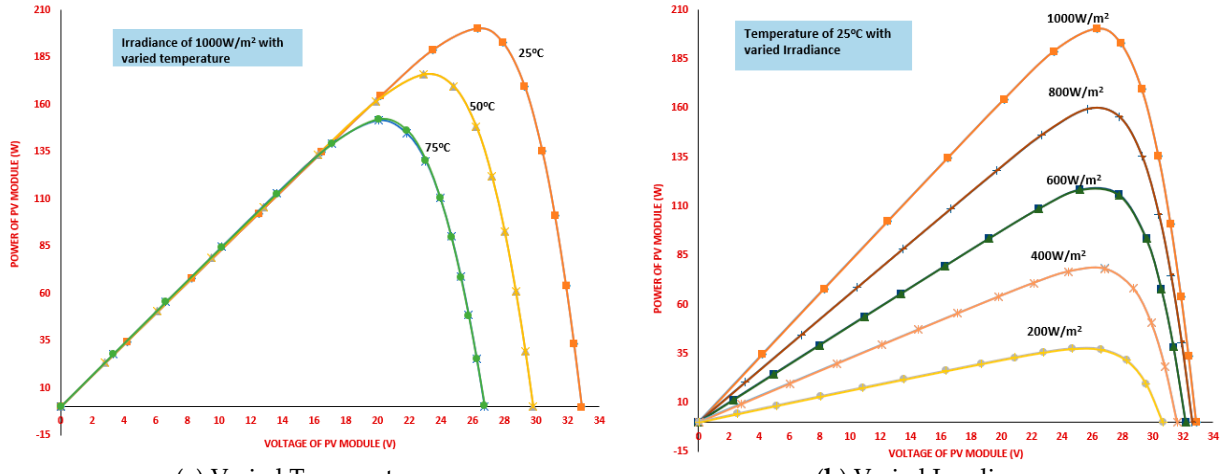
(**a**) Varied Temperature (**b**) Varied Irradiances

Figure 13. Acquired P–V characteristics for SD model of KC200GT PV module under various weather scenarios using MGA.



(**a**) Varied Temperature (**b**) Varied Irradiances

Figure 14. Acquired I–V characteristics for DD model of KC200GT PV module under various weather scenarios using MGA.



(**a**) Varied Temperature (**b**) Varied Irradiances

Figure 15. Acquired P–V characteristics for DD model of KC200GT PV module under various weather scenarios using MGA.

5. Conclusions

In this work, a novel MGA method for deriving parameters from SD and DD solar PV cell/panel models of RTC France and Kyocera KC200GT PV modules is given, taking into account PV manufacturing technology and solar cell modeling. The goal of the recommended MGA technique is to optimize the parameters for the best performance in terms of RMSE values. By obtaining the least four RMSE indicators with larger improvement percentages, the suggested MGA technique achieves significant superiority and statistical robustness in comparison to the recently described techniques. When determining the relevant PV parameters under fluctuating temperature and irradiance, the suggested MGA approach performs better than commercial PV systems. This shows the efficacy of the methodology and its capacity to produce fitted I–V data that are highly consistent with the manufacturer's data sheets. The exact solution of PV cell/panel models provides additional proof that the proposed MGA outperforms the optimizers recently published in the literature. The capacity of the suggested MGA technique to determine unknown PV properties is further illustrated by accounting for a range of operational conditions, including temperature and irradiance variations. The MGA optimizer consistently demonstrates superior performance in reducing RMSE compared to other algorithms across a range of weather conditions, with percentage improvements ranging from 8.07% to 90.29% for the SD and DD models.

Author Contributions: Conceptualization, W.A.; Methodology, M.G. and A.R.G.; Software, A.M.S.; Validation, A.M.S.; Formal analysis, W.A. and S.S.; Investigation, W.A. and M.G.; Data curation, M.G.; Writing—original draft, A.M.S. and A.R.G.; Writing—review & editing, S.S., A.M.S. and A.R.G.; Visualization, A.R.G.; Supervision, S.S. All authors have read and agreed to the published version of the manuscript.

Funding: King Abdulaziz University.

Data Availability Statement: The original contributions presented in the study are included in the article, further inquiries can be directed to the corresponding author.

Acknowledgments: The project was funded by the Deanship of Scientific Research (DSR) at King Abdulaziz University, Jeddah, under grant no. (GPIP: 1439-612-2024). The authors, therefore, acknowledge with thanks DSR for technical and financial support.

Conflicts of Interest: The authors declare no conflicts of interest. There are non-financial competing interests.

References

1. Li, S.; Gong, W.; Gu, Q. A Comprehensive Survey on Meta-Heuristic Algorithms for Parameter Extraction of Photovoltaic Models. *Renew. Sustain. Energy Rev.* **2021**, *141*, 110828. [CrossRef]
2. Abdel-Basset, M.; Mohamed, R.; Sharawi, M.; Abdel-Fatah, L.; Abouhawwash, M.; Sallam, K. A Comparative Study of Optimization Algorithms for Parameter Estimation of PV Solar Cells and Modules: Analysis and Case Studies. *Energy Rep.* **2022**, *8*, 13047–13065. [CrossRef]
3. Tyagi, V.V.; Rahim, N.A.A.; Rahim, N.A.; Selvaraj, J.A.L. Progress in Solar PV Technology: Research and Achievement. *Renew. Sustain. Energy Rev.* **2013**, *20*, 443–461. [CrossRef]
4. Singh, B.P.; Goyal, S.K.; Kumar, P. Solar Pv Cell Materials and Technologies: Analyzing the Recent Developments. *Mater. Today Proc.* **2021**, *43*, 2843–2849. [CrossRef]
5. Al-Ezzi, A.S.; Ansari, M.N.M. Photovoltaic Solar Cells: A Review. *Appl. Syst. Innov.* **2022**, *5*, 67. [CrossRef]
6. Solak, E.K.; Irmak, E. Advances in Organic Photovoltaic Cells: A Comprehensive Review of Materials, Technologies, and Performance. *RSC Adv.* **2023**, *13*, 12244–12269. [CrossRef]
7. Yuan, Y.; Tossoun, B.; Huang, Z.; Zeng, X.; Kurczveil, G.; Fiorentino, M.; Liang, D.; Beausoleil, R.G. Avalanche Photodiodes on Silicon Photonics. *J. Semicond.* **2022**, *43*, 021301. [CrossRef]
8. Shariah, A.; Mahasneh, F. Emitter Layer Optimization in Heterojunction Bifacial Silicon Solar Cells. *J. Semicond.* **2022**, *43*, 122701. [CrossRef]
9. Suresh Kumar, N.; Chandra Babu Naidu, K. A Review on Perovskite Solar Cells (PSCs), Materials and Applications. *J. Mater.* **2021**, *7*, 940–956. [CrossRef]
10. Jacak, J.E.; Jacak, W.A. Routes for Metallization of Perovskite Solar Cells. *Materials* **2022**, *15*, 2254. [CrossRef]
11. Xu, D.; Wu, P.; Tan, H. Self-assembled Monolayers for Perovskite Solar Cells. *Inf. Funct. Mater.* **2024**, *1*, 2–25. [CrossRef]

12. Zhang, T.; Luo, H.; Abdi-Jalebi, M.; Chen, H.; Zuo, L. Perovskite Solar Cells with Ferroelectricity. *J. Supercomput.* **2024**, *1*, 87–107. [CrossRef]
13. Li, X.; Ying, Z.; Wang, X.; Zeng, Y.; Yang, X.; Ye, J. How to Enable Highly Efficient and Large-Area Fabrication on Specific Textures for Monolithic Perovskite/Silicon Tandem Solar Cells? *Inf. Funct. Mater.* **2024**. *early view*. [CrossRef]
14. Hu, Y.; Li, Z.; Fang, X. Solution-Prepared AgBi2I7 Thin Films and Their Photodetecting Properties. *Wuji Cailiao Xuebao/J. Inorg. Mater.* **2023**, *38*, 1055–1061. [CrossRef]
15. Ding, X.D.; Zhou, X.W.; Meng, J.W.; Wang, H.X.; Wu, T.; Hua, Y.; Chen, C.; Cheng, M. NH4PF6 Assisted Buried Interface Defect Passivation for Planar Perovskite Solar Cells with Efficiency Exceeding 21%. *Rare Met.* **2023**, *42*, 3399–3409. [CrossRef]
16. Liu, S.P.; Qiu, X.C.; Guo, J.; Chen, P.A.; Liu, Y.; Wei, H.; Xia, J.N.; Xie, H.H.; Hu, Y.Y. Efficient P-Doping of P3HT for Hole Transporting Materials in Perovskite Solar Cells. *Rare Met.* **2022**, *41*, 2575–2581. [CrossRef]
17. Jiang, Z.Y.; Pan, M.; Ren, F.M.; Chen, R.; Sun, Z.X.; Yang, Z.C.; Liu, Z.H.; Chen, W. Boosting Stability of Inverted Perovskite Solar Cells with Magnetron-Sputtered Molybdenum Rear Electrodes. *Rare Met.* **2023**, *42*, 3741–3754. [CrossRef]
18. Hassan Hakmi, S.; Alnami, H.; Ginidi, A.; Shaheen, A.; Alghamdi, T.A.H. A Fractional Order-Kepler Optimization Algorithm (FO-KOA) for Single and Double-Diode Parameters PV Cell Extraction. *Heliyon* **2024**, *10*, e35771. [CrossRef]
19. Smaili, I.H.; Moustafa, G.; Almalawi, D.R.; Ginidi, A.; Shaheen, A.M.; Mansour, H.S. Enhanced Artificial Rabbits Algorithm Integrating Equilibrium Pool to Support PV Power Estimation via Module Parameter Identification. *Int. J. Energy Res.* **2024**, *2024*, 8913560. [CrossRef]
20. Ebrahimi, S.M.; Salahshour, E.; Malekzadeh, M. Francisco Gordillo Parameters Identification of PV Solar Cells and Modules Using Flexible Particle Swarm Optimization Algorithm. *Energy* **2019**, *179*, 358–372. [CrossRef]
21. Chen, X.; Yu, K.; Du, W.; Zhao, W.; Liu, G. Parameters Identification of Solar Cell Models Using Generalized Oppositional Teaching Learning Based Optimization. *Energy* **2016**, *99*, 170–180. [CrossRef]
22. Rizk, M. Rizk-Allah; A.El-Fergany, A. Emended Heap-Based Optimizer for Characterizing Performance of Industrial Solar Generating Units Using Triple-Diode Model. *Energy* **2021**, *237*, 121561. [CrossRef]
23. Ortiz-Conde, A.; García Sánchez, F.J.; Muci, J. New Method to Extract the Model Parameters of Solar Cells from the Explicit Analytic Solutions of Their Illuminated I–V Characteristics. *Sol. Energy Mater. Sol. Cells* **2006**, *90*, 352–361. [CrossRef]
24. Easwarakhanthan, T.; Bottin, J.; Bouhouch, I.; Boutrit, C. Nonlinear Minimization Algorithm for Determining the Solar Cell Parameters with Microcomputers. *Int. J. Sol. Energy* **1986**, *4*, 1–12. [CrossRef]
25. Kiani, A.T.; Nadeem, M.F.; Ahmed, A.; Khan, I.; Elavarasan, R.M.; Das, N. Optimal PV Parameter Estimation via Double Exponential Function-Based Dynamic Inertia Weight Particle Swarm Optimization. *Energies* **2020**, *13*, 4037. [CrossRef]
26. Li, S.; Gong, W.; Wang, L.; Yan, X.; Hu, C. A Hybrid Adaptive Teaching–Learning-Based Optimization and Differential Evolution for Parameter Identification of Photovoltaic Models. *Energy Convers. Manag.* **2020**, *225*, 113474. [CrossRef]
27. Restrepo-Cuestas, B.J.; Montano, J.; Ramos-Paja, C.A.; Trejos-Grisales, L.A.; Orozco-Gutierrez, M.L. Parameter Estimation of the Bishop Photovoltaic Model Using a Genetic Algorithm. *Appl. Sci.* **2022**, *12*, 2927. [CrossRef]
28. Long, W.; Jiao, J.; Liang, X.; Xu, M.; Tang, M.; Cai, S. Parameters Estimation of Photovoltaic Models Using a Novel Hybrid Seagull Optimization Algorithm. *Energy* **2022**, *249*, 123760. [CrossRef]
29. Kharchouf, Y.; Herbazi, R.; Chahboun, A. Parameter's Extraction of Solar Photovoltaic Models Using an Improved Differential Evolution Algorithm. *Energy Convers. Manag.* **2022**, *251*, 114972. [CrossRef]
30. Chen, X.; Yu, K. Hybridizing Cuckoo Search Algorithm with Biogeography-Based Optimization for Estimating Photovoltaic Model Parameters. *Sol. Energy* **2019**, *180*, 192–206. [CrossRef]
31. Shaheen, A.M.; El-Seheimy, R.A.; Xiong, G.; Elattar, E.; Ginidi, A.R. Parameter Identification of Solar Photovoltaic Cell and Module Models via Supply Demand Optimizer. *Ain Shams Eng. J.* **2022**, *13*, 101705. [CrossRef]
32. Al-Shamma'a, A.A.; Omotoso, H.O.; Alturki, F.A.; Farh, H.M.H.; Alkuhayli, A.; Alsharabi, K.; Noman, A.M. Parameter Estimation of Photovoltaic Cell/Modules Using Bonobo Optimizer. *Energies* **2021**, *15*, 140. [CrossRef]
33. Qais, M.H.; Hasanien, H.M.; Alghuwainem, S. Identification of Electrical Parameters for Three-Diode Photovoltaic Model Using Analytical and Sunflower Optimization Algorithm. *Appl. Energy* **2019**, *250*, 109–117. [CrossRef]
34. Abdel-Basset, M.; El-Shahat, D.; Chakrabortty, R.K.; Ryan, M. Parameter Estimation of Photovoltaic Models Using an Improved Marine Predators Algorithm. *Energy Convers. Manag.* **2021**, *227*, 113491. [CrossRef]
35. Long, W.; Wu, T.; Xu, M.; Tang, M.; Cai, S. Parameters Identification of Photovoltaic Models by Using an Enhanced Adaptive Butterfly Optimization Algorithm. *Energy* **2021**, *229*, 120750. [CrossRef]
36. Shaheen, A.M.; Elsayed, A.M.; Ginidi, A.R.; El-Sehiemy, R.A.; Elattar, E. Enhanced Social Network Search Algorithm with Powerful Exploitation Strategy for PV Parameters Estimation. *Energy Sci. Eng.* **2022**, *10*, 1398–1417. [CrossRef]
37. Fan, Y.; Wang, P.; Mafarja, M.; Wang, M.; Zhao, X.; Chen, H. A Bioinformatic Variant Fruit Fly Optimizer for Tackling Optimization Problems. *Knowl.-Based Syst.* **2021**, *213*, 106704. [CrossRef]
38. Abdel-Basset, M.; Mohamed, R.; El-Fergany, A.; Abouhawwash, M.; Askar, S.S. Parameters Identification of PV Triple-Diode Model Using Improved Generalized Normal Distribution Algorithm. *Mathematics* **2021**, *9*, 995. [CrossRef]
39. Li, S.; Gong, W.; Yan, X.; Hu, C.; Bai, D.; Wang, L. Parameter Estimation of Photovoltaic Models with Memetic Adaptive Differential Evolution. *Sol. Energy* **2019**, *190*, 465–474. [CrossRef]
40. Talatahari, S.; Azizi, M.; Gandomi, A.H. Material Generation Algorithm: A Novel Metaheuristic Algorithm for Optimization of Engineering Problems. *Processes* **2021**, *9*, 859. [CrossRef]

41. Ortiz-Conde, A.; Lugo-Muñoz, D.; García-Sánchez, F.J. An Explicit Multiexponential Model as an Alternative to Traditional Solar Cell Models with Series and Shunt Resistances. *IEEE J. Photovolt.* **2012**, *2*, 261–268. [CrossRef]
42. Chin, V.J.; Salam, Z.; Ishaque, K. Cell Modelling and Model Parameters Estimation Techniques for Photovoltaic Simulator Application: A Review. *Appl. Energy* **2015**, *154*, 500–519. [CrossRef]
43. Chin, V.J.; Salam, Z. Coyote Optimization Algorithm for the Parameter Extraction of Photovoltaic Cells. *Sol. Energy* **2019**, *194*, 656–670. [CrossRef]
44. Ginidi, A.; Ghoneim, S.M.; Elsayed, A.; El-Sehiemy, R.; Shaheen, A.; El-Fergany, A. Gorilla Troops Optimizer for Electrically Based Single and Double-Diode Models of Solar Photovoltaic Systems. *Sustainability* **2021**, *13*, 9459. [CrossRef]
45. Sulaiman, M.H.; Mustaffa, Z.; Saari, M.M.; Daniyal, H. Barnacles Mating Optimizer: A New Bio-Inspired Algorithm for Solving Engineering Optimization Problems. *Eng. Appl. Artif. Intell.* **2020**, *87*, 103330. [CrossRef]
46. Nematollahi, A.F.; Rahiminejad, A.; Vahidi, B. A Novel Physical Based Meta-Heuristic Optimization Method Known as Lightning Attachment Procedure Optimization. *Appl. Soft Comput. J.* **2017**, *59*, 596–621. [CrossRef]
47. Liang, J.; Ge, S.; Qu, B.; Yu, K.; Liu, F.; Yang, H.; Wei, P.; Li, Z. Classified Perturbation Mutation Based Particle Swarm Optimization Algorithm for Parameters Extraction of Photovoltaic Models. *Energy Convers. Manag.* **2020**, *203*, 112138. [CrossRef]
48. Şenel, F.A.; Gökçe, F.; Yüksel, A.S.; Yiğit, T. A Novel Hybrid PSO–GWO Algorithm for Optimization Problems. *Eng. Comput.* **2019**, *35*, 1359–1373. [CrossRef]
49. Hakmi, S.H.; Alnami, H.; Moustafa, G.; Ginidi, A.R.; Shaheen, A.M. Modified Rime-Ice Growth Optimizer with Polynomial Differential Learning Operator for Single- and Double-Diode PV Parameter Estimation Problem. *Electronics* **2024**, *13*, 1611. [CrossRef]
50. Yu, K.; Qu, B.; Yue, C.; Ge, S.; Chen, X.; Liang, J. A Performance-Guided JAYA Algorithm for Parameters Identification of Photovoltaic Cell and Module. *Appl. Energy* **2019**, *237*, 241–257. [CrossRef]
51. Rizk-Allah, R.M.; El-Fergany, A.A. Conscious Neighborhood Scheme-Based Laplacian Barnacles Mating Algorithm for Parameters Optimization of Photovoltaic Single- and Double-Diode Models. *Energy Convers. Manag.* **2020**, *226*, 113522. [CrossRef]
52. Ali, E.E.; El-Hameed, M.A.; El-Fergany, A.A.; El-Arini, M.M. Parameter Extraction of Photovoltaic Generating Units Using Multi-Verse Optimizer. *Sustain. Energy Technol. Assess.* **2016**, *17*, 68–76. [CrossRef]
53. Chen, H.; Jiao, S.; Wang, M.; Heidari, A.A.; Zhao, X. Parameters Identification of Photovoltaic Cells and Modules Using Diversification-Enriched Harris Hawks Optimization with Chaotic Drifts. *J. Clean. Prod.* **2020**, *244*, 118778. [CrossRef]
54. Khanna, V.; Das, B.K.; Bisht, D.; Vandana; Singh, P.K. A Three Diode Model for Industrial Solar Cells and Estimation of Solar Cell Parameters Using PSO Algorithm. *Renew. Energy* **2015**, *78*, 105–113. [CrossRef]
55. Kanimozhi, G.; Kumar, H. Modeling of Solar Cell under Different Conditions by Ant Lion Optimizer with LambertW Function. *Appl. Soft Comput. J.* **2018**, *71*, 141–151. [CrossRef]
56. Ben Aribia, H.; El-Rifaie, A.M.; Tolba, M.A.; Shaheen, A.; Moustafa, G.; Elsayed, F.; Elshahed, M. Growth Optimizer for Parameter Identification of Solar Photovoltaic Cells and Modules. *Sustainability* **2023**, *15*, 7896. [CrossRef]
57. Beigi, A.M.; Maroosi, A. Parameter Identification for Solar Cells and Module Using a Hybrid Firefly and Pattern Search Algorithms. *Sol. Energy* **2018**, *171*, 435–446. [CrossRef]
58. Moustafa, G.; Smaili, I.H.; Almalawi, D.R.; Ginidi, A.R.; Shaheen, A.M.; Elshahed, M.; Mansour, H.S.E. Dwarf Mongoose Optimizer for Optimal Modeling of Solar PV Systems and Parameter Extraction. *Electronics* **2023**, *12*, 4990. [CrossRef]

Disclaimer/Publisher's Note: The statements, opinions and data contained in all publications are solely those of the individual author(s) and contributor(s) and not of MDPI and/or the editor(s). MDPI and/or the editor(s) disclaim responsibility for any injury to people or property resulting from any ideas, methods, instructions or products referred to in the content.